R-1113

OPTIMAL SOLAR SAIL PLANETOCENTRIC TRAJECTORIES

by

Lester L. Sackett

September 1977

The Charles Stark Draper Laboratory, Inc.
Cambridge, Massachusetts 02139

TECHNICAL REPORT STANDARD TITLE PAGE

1. Report No.	2. Government Accession No.	3. Recipient's Catalog No.

4. Title and Subtitle	5. Report Date
Optimal Solar Sail Planetocentric Trajectories	September 1977
	6. Performing Organization Code
7. Author(s) Lester L. Sackett	8. Performing Organization Report No. R-1113
9. Performing Organization Name and Address The Charles Stark Draper Lab 555 Technology Sq. Cambridge, Mass. 02139	10. Work Unit No.
	11. Contract or Grant No. NAS 7-100
	13. Type of Report and Period Covered Contract Report
12. Sponsoring Agency Name and Address NASA Washington, DC	14. Sponsoring Agency Code

15. Supplementary Notes
Technical Monitor, David B. Smith
Jet Propulsion Laboratory, Pasadena, CA

16. Abstract

This report describes the analysis of solar sail planetocentric optimal trajectory problem. A computer program has been produced to calculate optimal trajectories for a limited performance analysis. A square sail model is included and some consideration is given to a heliogyro sail model. Orbit to a subescape point and orbit to orbit transfer are considered. Trajectories about the four inner planets can be calculated and shadowing, oblateness, and solar motion may be included. Equinoctial orbital elements are used to avoid the classical singularities, and the method of averaging is applied to increase computational speed. Solution of the two-point boundary-value problem which arises from the application of optimization theory is accomplished with a Newton procedure. Time optimal trajectories are emphasized, but a penalty function has been considered to prevent trajectories which intersect a planet's surface. A number of example cases are presented which illustrate typical solar sail performance.

17. Key Words Suggested by Author	18. Distribution Statement
solar sail, optimal trajectories, orbit transfer, low thrust, heliogyro	unclassified - unlimited

19. Security Classif. (of this report)	20. Security Classif. (of this page)	21. No. of Pages	22. Price
Unclassified	Unclassified		

R-1113

OPTIMAL SOLAR SAIL PLANETOCENTRIC TRAJECTORIES

by

Lester L. Sackett

September 1977

Approved: Norman E. Sears

Norman E. Sears

The Charles Stark Draper Laboratory, Inc.

Cambridge, Massachusetts 02139

ACKNOWLEDGMENT

This report was prepared under Project 51-77200 sponsored by the Jet Propulsion Laboratory under NASA Contract NAS 7-100 and JPL subcontract 954724. The technical monitor was Mr. David B. Smith.

The author wishes to acknowledge the important contribution of Theodore N. Edelbaum, a participant in this study until his death in April 1977. He was a pioneer in the field of astrodynamics and trajectory optimization and a principal contributor to this study and its precursors.

The author would also like to thank David Smith and Jerome Wright of JPL for their help and encouragement and Andrew Green and Louis D'Amario of Draper Lab for advice and assistance. Kent Sharp, formerly of Draper Lab, contributed valuable programming support.

TABLE OF CONTENTS

SECTION 1

INTRODUCTION

The concept of using a solar sail as a means of transportation within the solar system was first discussed seriously in the United States in the 1950's.[1] Recently, the possibility of using a solar sail has been given serious consideration.[2] The earliest contender for an actual mission would be a rendezvous with Halley's comet in 1986, with a launch in 1982. After that a solar sail could be used for a variety of solar system missions including, for example, a Mars sample return. However, recent NASA decisions indicate that the solar sail will not be developed for near term missions. Some possible missions would include a planetary escape or capture segment of the trajectory in addition to a heliocentric trajectory segment. The thrust acceleration level for sail designs in the near term are low, on the order of 1 mm/s^2, and so escape or capture requires a spiral phase from a low orbit to escape or from initial capture to a lower orbit. Typically there would be several dozen or even hundreds of orbits. This system is similar to other low thrust systems such as electric propulsion. The principal subjects of this report are the spiral phase of a planetary escape trajectory and orbit to orbit transfer. A computer program has been developed to calculate solar sail planetary trajectories to a near escape point. It can also be used to calculate spirals to a lower orbit and for trajectories about Mercury, Venus, and Mars as well as Earth.

A solar sail consists of a large area of reflective material. Typically, a very thin plastic is coated with a reflective metallic surface. Sunlight reflecting off the surface imparts a force which is approximately normal to the surface. The pressure exerted on a perfectly reflecting sail normal to the sun at 1 A.U. is 0.9 N/m^2. By varying the angle of the surface with the photon direction, the force direction can be changed, although there will never be a component of force toward the sun. If the sail has a large enough

area, and the total vehicle is light enough, then reasonable accelerations will result. In heliocentric space it is possible to thrust so that the sail moves away from the sun by having a component of the reflective force in the direction of motion. If the force has a component in the direction opposite to the motion, the total angular momentum will be decreased and the sail vehicle will fall in toward the sun. When the sail is in orbit about a planet, the sail direction can be varied so that the thrust almost always has a component in the direction of motion and so will increase the semimajor axis or energy even when the vehicle is moving toward the sun in its planetocentric orbit. Typically, planetary orbits have periods of only a few hours or days and, therefore, the necessary sail angle with respect to the sun direction to obtain desired force directions may be changing rapidly. In practice there are constraints on how fast these sail angles can be changed. These constraints are considered only in a limited fashion in this report.

The Jet Propulsion Laboratory has considered two sail models as possible interplanetary propulsion systems: a square sail and the heliogyro. More recently a decision was made to concentrate study on the heliogyro model. This report stresses the square sail model which was implemented in the computer code. A heliogyro model is discussed which is similar to the square sail model, but which was not implemented.

The square sail is a large (about 850m X 850m), nearly flat sheet with attendant structure, one side reflective and one side dark. The heliogyro consists of a central hub with 12 blades, 6 each in two parallel planes, each blade about 6 km long and several meters wide. The heliogyro would spin with a period of about three minutes. Rigidity is provided by the centrifugal force. Variations in thrust direction as well as torques for attitude changes are accomplished by varying the blade pitch, that is, the angle about the longitudinal axis of the blade.

The purpose of this study was to develop a program to produce optimal planeocentric solar sail trajectories and to apply that program to a performance analysis. Earlier papers ahve considered nonoptimal planetary trajectories. Sands[3] considered a two-dimensional escape maneuver for a trajectory plane containing the sun-planet line for the idealized flat sail, perfectly reflecting specularly on both sides. The sail is assumed to rotate about its axis at half the

rate of revolution about the planet. Fimple[4] considered the three-dimensional case of a sail vehicle in orbit about a planet with the orbital plane normal to the sun-planet line, also for the idealized sail. The sail angle is chosen so that the component of thrust in the direction of motion is maximized. Quasi-circular orbits result until near escape. Neither Sands nor Fimple included solar motion. Time optimal helicentric trajectories have been calculated for the idealized sail. Zhukov and Lebedev[5] considered planar trajectories. Sauer[6] generalized this work to three-dimensional trajectories. MacNeil[7] conceived of the heliogyro design and with others produced additional studies.[8,9,10]

The study reported here built upon a computer program (SECKSPOT) which had been developed to produce electric propulsion geocentric orbit transfers.[11,12] The program uses: (1) the method of averaging[13] in order to reduce the amount of computer time needed to calculate many trajectories, each of which includes many orbits about a planet, and (2) equinoctial orbital elements which are nonsingular for zero eccentricity and inclination.[14] Since averaging is valid only if the thrust to local weight ratio is small, the scheme cannot by itself yield trajectories to escape energy (infinite semimajor axis). The scheme can be used to calculate trajectories to a large semimajor axis (small magnitude but negative energy). The effect of shadowing by the planet may be included as well as oblateness for Earth trajectories. The solar sail program (called SUNSPOT for SUN-Sail Program for Optimal Trajectories) does not include planetshine or drag effects which may be important at low altitudes. Although attitude constraints may be important for some trajectories, they were not included explicitly in the optimization procedure.

Kryloff-Bogoliuboff averaging of both the state and costate is used. The averaged rates of change of the mean values of the state and costate are found by numerical quadrature. The differential equations for the mean state and costate may then be integrated in large time steps (typically days). The method of averaging has been used extensively in recent years. Edelbaum[15,16] has used averaging to calculate analytic solutions for special cases of optimal low thrust trajectories, and others have used averaging when considering effects such as oblateness, third body perturbations and non-optimal thrusting.[17,18,19] Jasper[20] utilizes equinoctial orbital elements and averaging in low thrust optimization work. The effect

of oblateness is included by analytically adding its associated rate of change of the mean state and costate to that due to thrust. The effects of shadowing are calculated by assuming that there is no solar radiation pressure when the sail is in shadow.

The overall trajectory is optimized by a shooting method. Initial values of the unspecified states and costates are chosen at the initial time. An optimum low thrust trajectory is then generated by integrating the state and costate until the final time. This will generate an optimal trajectory to the wrong terminal state. A sensitivity matrix is then generated by varying the initial conditions and running a set of neighboring trajectories. A Newton iteration on the initial conditions is then used to drive the terminal errors to within specified bounds. The final converged trajectory is a minimum time trajectory (except when a penalty function is added to the cost to prevent subterranean trajectories, in which case nearly minimum time trajectories result).

A computer program has been developed to calculate planetocentric solar sail trajectories. The analysis and code can be used in a performance analysis. A limited set of cases are discussed in the result section of this report. A paper based on the material in this report has been presented.[21] Related work for trajectories beginning at large semimajor axis and continuing to escape energy performed by Green is reported in Ref. 22. The results of the work reported here and of the work by Green include the first production of optimal solar sail planetocentric trajectories.

In the next section some of the general techniques used are discussed. The following section contains the main analytical contribution of this study. A number of trajectories are given in the result section, constituting a partial performance analysis. A preliminary heliogyro model is discussed in Appendix A. Results from previous efforts which are needed for the sail program are given in Appendices B - D. As part of the solar sail effort, preliminary results yielded non-optimal near escape trajectories using a maximum energy strategy. These results were reported to JPL during the course of the work, but are summarized in Appendix E.

SECTION 2

GENERAL TECHNIQUE

2.1 Introduction

Three areas of general technique are discussed in this section. One is the method of averaging, essential to the running of a program which generates many trajectories in a reasonable amount of computer time. Second is discussed the method of generation of the final trajectory. A time optimal trajectory is desired. A state and costate formulation is used which results in a two-point boundary-value problem which can be solved by a Newton iteration procedure. Finally some comments on numerical techniques are made.

2.2 Averaging

A great savings in computer time can be effected by considering a first approximation to the state and costate. Short period variations in the state and costate are eliminated by the averaging technique. When low thrust propulsion is utilized and the other perturbations to the inverse square motion are small and when the state includes the five slowly varying orbital elements which indicate the size, shape and orientation of an orbit and possibly other slowly varying quantities, then averaging may be used. The orbital element indicating the position of the spacecraft in the orbit is eliminated by the averaging process.

The averaged Hamiltonian can be defined as

$$\bar{H} = \frac{1}{T} \int_{t-\frac{T}{2}}^{t+\frac{T}{2}} H \, dt \qquad (2.1)$$

where H is the unaveraged Hamiltonian and T is the orbital period. When calculating this integral the state and costate are held fixed. The motion of the spacecraft is assumed to vary in a manner described by Kepler's equation over the averaging integration. The approximate state and costate satisfy the canonical equations.

$$\dot{\bar{x}}^T = \frac{\partial \tilde{H}}{\partial \bar{\lambda}} \tag{2.2}$$

$$\dot{\bar{\lambda}}^T = -\frac{\partial \tilde{H}}{\partial \bar{x}} \tag{2.3}$$

where the overbar indicates the approximate quantities.

In what follows the averaging integral for oblateness (J_2) is solved analytically; otherwise a numerical quadrature formula is used. The differential equations can then be solved numerically using a time step which is much larger than but unrelated to the number of orbital revolutions.

2.3 Solution of Boundary Value Problem

The method used to generate a low thrust trajectory is to develop the Hamiltonian, to calculate a control (the thrust direction) and to write the canonical equations for the state and costate. The initial state is specified. Application of transversality conditions for the time optimal problem yield additional specifications on the state and costate. Thus a two-point boundary-value problem results which must be solved to obtain the requisite trajectory. When these equations are solved, an extremal trajectory will result which is usually locally optimal. No attempt is made to investigate generalized Jacobi-type conditions to establish local sufficiency. Also, in common with other nonlinear problems, there may be more than one extremal meeting the same end conditions. The very difficult question of global optimality is not considered.

The single trajectory generation portion of the code is coupled with a Newton iterator to solve the two-point boundary-value problem. The unknown initial conditions and value of the final time are iterated on in order to meet the final conditions which are functions of the final state and costate. The partial derivative matrix of final conditions with respect to the initial costate is obtained numerically by calculating neighboring trajectories to a nominal.

The Newton method works by first guessing values for the iteration parameters, call them $\underline{x}$ and t_f, and then running a nominal trajectory which will yield final conditions $\underline{y}$ which in general are not equal to the desired final conditions, y_d. Revised values for $\underline{x}$, t_f may then

be obtained by calculating a sensitivity matrix or partial derivative matrix, A, which is generated by varying slightly, one at a time, each of the iteration parameters, $\underline{x}$, and running a new, neighboring, trajectory. Differencing the resulting values of the final conditions with the nominal values yields a Δy for each Δx_i. In addition $\frac{\partial y}{\partial t_f}$ can be calculated analytically except perhaps for $\frac{\partial H}{\partial t_f}$ which can be approximated numerically by varying t_f slightly and evaluating the corresponding H, differencing this with the nominal H and dividing by Δt_f. Then A is an approximation for the partial of $\underline{y}$ with respect to $\underline{x}$, t_f.

$$A = \begin{bmatrix} \frac{\Delta \underline{y}^T}{\Delta \underline{x}} \\ \\ \frac{\partial \underline{y}^T}{\partial t_f} \end{bmatrix} \tag{2.4}$$

A revised estimate of the iteration parameters can then be obtained by the formula

$$\begin{bmatrix} \underline{x} \\ t_f \end{bmatrix}_{NEW} = \begin{bmatrix} \underline{x} \\ t_f \end{bmatrix}_{OLD} - A^{-1}(\underline{y}-\underline{y}_d) \tag{2.5}$$

A new nominal trajectory can then be generated and the procedure continued until the final conditions are met to within some tolerance. In the event that the new $\underline{x}$, t_f do not yield a reduction in the norm of the final condition errors, the change in ($\underline{x}$, t_f) is reduced in magnitude by factors of 2. Also there is an option of using a modified Newton-Raphson procedure wherein the A matrix is not always recalculated at each iteration by running neighboring trajectories, but instead a new A may be approximated using the old A and the values of the changes in $\underline{x}$, t_f.

2.4 Numerical Methods

A Newton-Raphson iterator is used which calculates the sensitivity matrix by running neighboring trajectories by changing slightly the initial values of the iteration parameters, one at a time. The size of the change in the iteration variables is chosen by the user and can affect the accuracy of the matrix. A Modified Newton-Raphson iterator used basically the same technique but many of the iterations make use of a modified sensitivity matrix rather than calculating a new one by running neighboring trajectories at each iteration.

The low thrust differential equations are integrated using a fourth order Runge-Kutta method. The time step is selected by the user. Cutting the size of the time step can increase the accuracy of the trajectory but rapidly increase run time.

Numerical averaging utilizes a Gaussian quadrature. The number of points sampled on an orbit can largely be determined by the user. Again, more points increase accuracy at the expense of run time.

SECTION 3

ANALYSIS

3.1 Sail Force Model

A square sail force model was implemented in the computer code and this section stresses that model. Limited heliogyro data was supplied by JPL and preliminary modeling effort is discussed in Appendix A. This effort was not included in the computer code. A simple model of the heliogyro would be similar to that given in this section.

The acceleration exerted by the photon pressure of sunlight on a flat, perfectly reflecting surface, whose normal has an angle, α, with the sun direction, has a direction along the normal to the back of the sail and a magnitude given by

$$a_F = \frac{a_c}{R^2} \cos^2\alpha \qquad (3.1)$$

where a_c, the characteristic acceleration, is the acceleration at 1 A.U. caused by the photons reflecting off a sail whose surface is normal to the sun-line; R is the distance from the sun in A.U.'s. If $\hat{\underline{R}}$ is the unit vector from sun to space vehicle and $\hat{\underline{n}}$ the unit normal to the sail back, the acceleration can be written

$$\underline{a}_F = \frac{a_c}{R^2} (\hat{\underline{n}}^T \hat{\underline{R}})^2 \hat{\underline{n}} \qquad (3.2)$$

since $\cos\alpha = \hat{\underline{n}}^T \hat{\underline{R}}$. This expression represents the model that has been used in much of the previously reported work (e.g., Ref. 3, 4, 5, 6).

The square sail model which was under consideration was not perfectly flat, nor was the reflection purely specular. The framework produced a kite-like structure. The sail was bowed somewhat with an

apex at the center. There was some absorption and some emission from both front and back. To more accurately model these effects, an expansion in cos θ, where θ is the angle between the force vector and the sun-line, was fit to more precise data for the geometry and reflective characteristics of the sail model by the Jet Propulsion Laboratory.[23] The following relationship was produced:

$$\underline{a}_F = \frac{a_c}{R^2} (c_1 + c_2 \cos 2\theta + c_3 \cos 4\theta)\hat{\underline{u}} \qquad (3.3)$$

where $\hat{\underline{u}}$ is a unit vector in the force direction, not necessarily parallel with the normal to sail surface. The thrust direction $\hat{\underline{u}}$ could be written as a function of two angles, the cone angle, θ, where $\cos \theta = \hat{\underline{R}}^T\hat{\underline{u}}$ and the clock angle, which is the angle between projections of a reference direction and the thrust direction onto a plane normal to the sun-line (see Figure 3-1). The expression in Eq. (3.3) could also be expressed as a

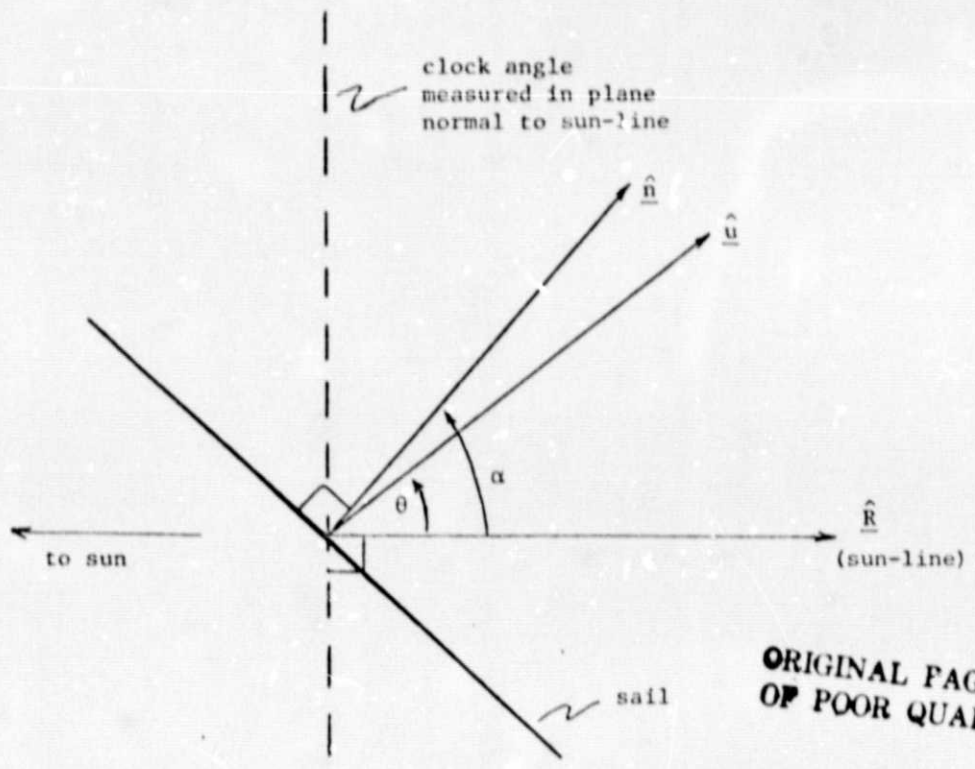

Figure 3-1. Sail geometry (in the plane of the sun-line and force vector).

function of $\cos^2\theta$ and $\cos^4\theta$. The parameters c_1, c_2, c_3 are constants which depend on the shape and reflective qualities of the sail. Note that if $c_1 = c_2 = 0.5$ and $c_3 = 0$, then the expression reduces to $\cos^2\theta$, which corresponds to the idealized square sail. The relationship between a body-fixed coordinate frame and θ may be obtained but is not necessary for our purposes.

One model produced by JPL had coefficients given by $c_1 = 0.367$, $c_2 = 0.643$, and $c_3 = -0.010$. The locus of the tip of the normalized force vector for these coefficients and also for the idealized sail coefficients is plotted in Figure 3-2. A line drawn from the origin at an angle θ with the horizontal axis and terminating at the curve will

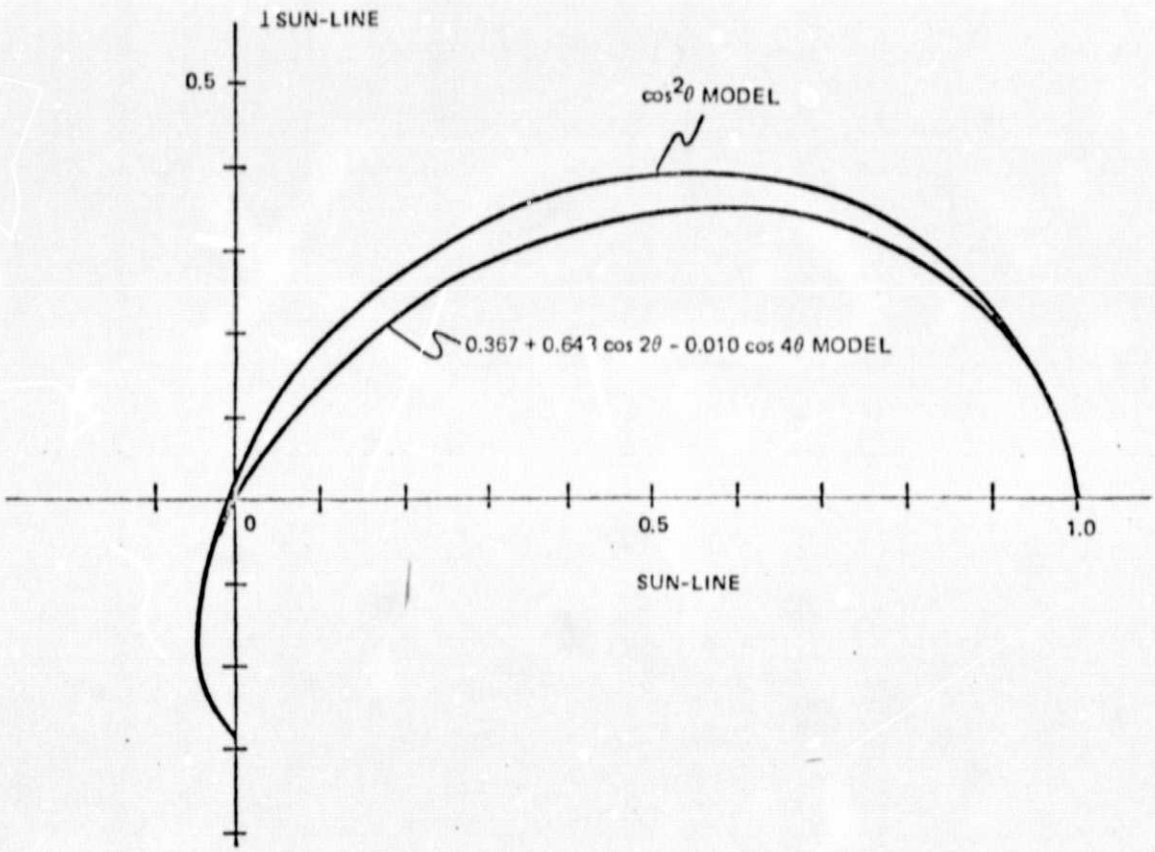

Figure 3-2. Locus of tip of force vector as cone angle varies.

have a length representing the force magnitude. The maximum force magnitude is one, which occurs when the force vector is parallel to the sunline. At $\theta = 62.585°$ the force magnitude is zero for the nonidealized sail. This is the cutoff angle. For θ greater than this angle, the equation dictates a negative force magnitude.

The force model of Eq. (3.3) is only an approximation and its behavior for β approaching 180° is not realistic. If $c_3 \neq 0$, then for some $\theta < 90°$, $b(\theta) = 0$ and for larger θ, b is negative implying a force toward the sun, which is impossible. The θ at which $b(\theta) = 0$ was considered a cutoff point and any θ which resulted from the mathematical optimization greater than this cutoff was reset to the cutoff value. The cutoff value may be obtained by setting $b(\theta) = 0$ and solving for θ analytically, as a function of c_1, c_2, and c_3.

In order to calculate the cutoff angle it is convenient to transform Eq. (3.3) to an expression in $\cos^2\theta$ and $\cos^4\theta$, i.e.

$$b(\theta) = k_1 + k_2 \cos^2\theta + k_3 \cos^4\theta \tag{3.4}$$

From trigonometric identities:

$$\begin{aligned} k_1 &= c_1 - c_2 + c_3 \\ k_2 &= 2c_2 - 8c_3 \\ k_3 &= 8c_3 \end{aligned} \tag{3.5}$$

For $b(\theta) = 0$

$$\cos^2\theta = \frac{-k_2 \pm \sqrt{k_2^2 - 4k_1k_3}}{2k_3} \tag{3.6}$$

The coefficient k_2 was always positive and much larger than k_1 and k_3 so that the positive square root is the correct root. Thus, the cutoff value of θ is given by

$$\theta_c = \cos^{-1}\left\{\sqrt{\frac{-k_2 + \sqrt{k_2^2 - 4k_1k_3}}{2k_3}}\right\} \tag{3.7}$$

where θ_c is between 0° and 90° (in the computer code 0 and, therefore, θ_c was assumed to lie between 90° and 180°; thus, the sign on the outer square root was negative). If $k_3 = 0$, the cut-off angle is simply obtained.

3.2 The Equations of Motion in Equinoctial Orbital Elements

A variation of parameter formulation using equinoctial orbital elements was used for the equations of motion. By using equinoctial orbital elements the singularities that occur for zero eccentricity or inclinations of zero or ninety degrees when using classical orbital elements are avoided. (For inclinations near 180°, retrograde equinoctial orbital elements can be used, although we will not consider that case in this report.)

The direct equinoctial orbital elements are defined in terms of the classical orbital elements by the formulas

$$\begin{aligned} a &= a \\ h &= e \sin(\omega + \Omega) \\ k &= e \cos(\omega + \Omega) \\ p &= \tan\left(\frac{i}{2}\right) \sin\Omega \\ q &= \tan\left(\frac{i}{2}\right) \cos\Omega \end{aligned} \qquad (3.8)$$

where a is the semimajor axis, e is the eccentricity, i is the inclination, Ω is the longitude of the ascending node, ω is the argument of pericenter. A sixth parameter, F, called the eccentric longitude, indicates the position in an orbit. It is given in terms of the classical variables by

$$F = E + \Omega + \omega \qquad (3.9)$$

where E is the eccentric anomaly. The variable F will be eliminated by the averaging process. Further details about equinoctial elements are given in Refs. 12, 17 and 24.

The inverse relationships are defined by

$$\begin{aligned} a &= a \\ e &= (h^2 + k^2)^{1/2} \end{aligned}$$

$$
\begin{aligned}
i &= 2\tan^{-1}(\sqrt{p^2 + q^2}) \\
\Omega &= \tan^{-1}(p/q) \\
\omega &= \tan^{-1}(h/k) - \tan^{-1}(p/q)
\end{aligned}
\tag{3.10}
$$

The equinoctial coordinate frame is defined by the basis vectors $\hat{\underline{f}}$, $\hat{\underline{g}}$, $\hat{\underline{w}}$, which are given below with respect to an inertial coordinate frame.

$$
\hat{\underline{f}} = \frac{1}{1 + p^2 + q^2} \begin{bmatrix} 1 - p^2 + q^2 \\ 2pq \\ -2p \end{bmatrix}
$$

$$
\hat{\underline{g}} = \frac{1}{1 + p^2 + q^2} \begin{bmatrix} 2pq \\ 1 + p^2 - q^2 \\ 2q \end{bmatrix} \tag{3.11}
$$

$$
\hat{\underline{w}} = \frac{1}{1 + p^2 + q^2} \begin{bmatrix} 2p \\ -2q \\ 1 - p^2 - q^2 \end{bmatrix}
$$

This coordinate frame is illustrated in Figure 3-3 where $\hat{\underline{w}}$ is normal to the orbital plane.

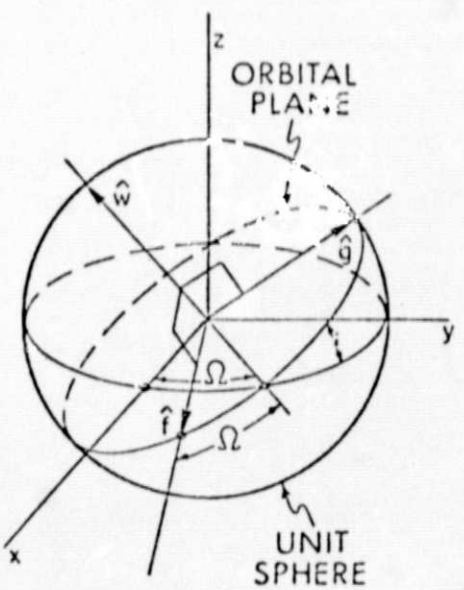

Figure 3-3. The equinoctial coordinate frame.

The mean longitude is defined by

$$\lambda = M + \omega + \Omega \tag{3.12}$$

The eccentric longitude, F, was defined in Eq. (3.9). Kepler's equation in terms of λ and F is then given by

$$\lambda = F - k \sin F + h \cos F \tag{3.13}$$

Position and velocity are given by

$$\underline{r} = X_1 \hat{\underline{f}} + Y_1 \hat{\underline{g}} \tag{3.14}$$

$$\dot{\underline{r}} = \dot{X}_1 \hat{\underline{f}} + \dot{Y}_1 \hat{\underline{g}} \tag{3.15}$$

where

$$X_1 = a[(1 - h^2\beta) \cos F + hk\beta \sin F - k] \tag{3.16}$$

$$Y_1 = a[(1 - k^2\beta) \sin F + hk\beta \cos F - h] \tag{3.17}$$

$$\dot{X}_1 = \frac{na^2}{r} [hk\beta \cos F - (1 - h^2\beta) \sin F] \tag{3.18}$$

$$\dot{Y}_1 = \frac{na^2}{r} [(1 - k^2\beta) \cos F - hk\beta \sin F] \tag{3.19}$$

and

$$n = \frac{\mu}{a^3} \tag{3.20}$$

$$\frac{r}{a} = 1 - k \cos F - h \sin F \tag{3.21}$$

μ is the gravitational constant and

$$\beta = \frac{1}{1 + \sqrt{1 - h^2 - k^2}} \tag{3.22}$$

The unaveraged variation of parameters formula for an object in an inverse square gravitational field perturbed by a force $\underline{u}$ is

$$\dot{\underline{Z}} = M(\underline{Z},F)\ \underline{u} \tag{3.23}$$

where $\underline{Z}$ represents the five equinoctial orbital elements (a, h, k, p, q). We define the 5 × 3 matrix

$$M(\underline{Z},F) = \frac{\partial \underline{Z}}{\partial \dot{\underline{r}}} \tag{3.24}$$

The elements of this matrix are given in Table B-1 of Appendix B.

3.3 The Optimization Problem

It is desired to calculate minimum time trajectories for escape, capture, and orbit to orbit transfer. The orbital element and averaging techniques did not permit trajectories to escape energy when eccentricity goes to one and the thrust to weight ratio becomes too large. For planetary escape the final state condition is that energy be zero. This is equivalent to infinite semimajor axis. Because of the limitations of the technique, trajectories to a subescape condition are considered. This is defined as a large, but finite semimajor axis, or equivalently as a small magnitude, negative energy. The initial orbit is assumed to be given. For orbit transfer the initial orbit is given, and either the final orbit is completely specified or else three orbital elements (a, e, i) are specified. The capture problem is considered a special case of the orbit transfer problem, since a zero energy initial orbit cannot be assumed. Thus a quasi-capture trajectory problem assumes that the initial orbit is given and that the final orbit is at some lower energy requiring a spiral trajectory downward.

A calculus of variations or maximum principal approach is used. The initial time and state are given; some subset of the final state is given. The state equations are given by Eq. (3.23) with the force given by Eq. (3.3). In summary

$$\dot{\underline{Z}} = \frac{a_c}{R^2}\, b(e)\ M(\underline{Z},\underline{F})\ \hat{\underline{u}} \tag{3.25}$$

where

$$b(\theta) = c_1 + c_2 \cos 2\theta + c_3 \cos 4\theta \tag{3.26}$$

and

$$\cos\theta = \hat{\underline{R}}^T \hat{\underline{u}} \tag{3.27}$$

and c_1, c_2, c_3 are constants. The distance to the sun is a function of time and the direction $\hat{\underline{R}}$ depends on the state when using an equinoctial coordinate frame. The characteristic acceleration, a_c, is a given constant. The control is the force direction $\hat{\underline{u}}$.

The unaveraged Hamiltonian is given by

$$H = \underline{\lambda}^T \dot{\underline{Z}} = \frac{a_c}{R^2} b(\theta)\, \underline{\lambda}^T M \hat{\underline{u}} \tag{3.28}$$

Applying the method of averaging, define the averaged Hamiltonian as

$$\tilde{H} = \frac{1}{T_o} \int_{\tau - \frac{T_o}{2}}^{\tau + \frac{T_o}{2}} H(\underline{Z}, \underline{\lambda}, F(t), t, \hat{\underline{u}})\, dt \tag{3.29}$$

where T_o is the orbital period. It is convenient to perform the integration with respect to the eccentric longitude, F. Then

$$\tilde{H} = \frac{1}{T_o} \int_{-\pi}^{\pi} H(\underline{Z}, \underline{\lambda}, F, t, \hat{\underline{u}}) \left(\frac{dt}{dF}\right) dF \tag{3.30}$$

where

$$\frac{dt}{dF} = \frac{T_o}{2\pi} (1 - \bar{k} \cos F - \bar{h} \sin F) \tag{3.31}$$

For convenience define

$$s(\underline{Z}, F) = \frac{1}{T_o} \frac{dt}{dF} \tag{3.32}$$

The overbar indicates that the quantities are held constant during the averaging interval. The $\bar{t}$ dependence is time dependence which does not depend on the spacecraft location such as the planet - sun position.

Necessary conditions for an optimal trajectory are that the Euler-Lagrange equations be satisfied:

$$\dot{\bar{Z}} = \frac{\partial H^T}{\partial \bar{\lambda}} = \int_{-\pi}^{\pi} \frac{\partial H^T}{\partial \bar{\lambda}} \, s \, dF \tag{3.33}$$

$$\dot{\bar{\lambda}}^T = - \frac{\partial H}{\partial \bar{Z}} = - \int_{-\pi}^{\pi} \left(\frac{\partial H}{\partial \bar{Z}} \, s + H \frac{\partial s}{\partial \bar{Z}} \right) dF \tag{3.34}$$

where

$$\frac{\partial H^T}{\partial \bar{\lambda}} = \dot{\bar{Z}} \, (\bar{Z}, F, \hat{u}, \bar{t}) \tag{3.35}$$

$$\frac{\partial H}{\partial \bar{Z}_i} = \bar{\lambda}^T \frac{\partial \dot{\bar{Z}}}{\partial \bar{Z}_i}$$

$$= \frac{a_c}{R^2} \, \bar{\lambda}^T \left\{ \frac{\partial b}{\partial \bar{Z}_i} \, M + b \frac{\partial M}{\partial \bar{Z}_i} \right\} \hat{u} \, s \tag{3.36}$$

$$\frac{\partial s}{\partial \bar{Z}} = \frac{1}{2\pi} \begin{bmatrix} 0 \\ - \sin F \\ - \cos F \\ 0 \\ 0 \end{bmatrix} \tag{3.37}$$

$\frac{\partial M}{\partial \bar{Z}}$ is given in Appendix B.

From Eqs. (3.26) and (3.27)

$$\frac{\partial b}{\partial \underline{Z}} = \frac{\partial b}{\partial \theta} \frac{\partial \theta}{\partial \underline{Z}} \tag{3.38}$$

where

$$\frac{\partial b}{\partial \theta} = -2c_2 \sin 2\theta - 4c_3 \sin 4\theta \tag{3.39}$$

and

$$\frac{\partial \theta}{\partial \underline{Z}} = -\frac{1}{\sin\theta} \hat{\underline{u}}^T \frac{\partial \hat{\underline{R}}}{\partial \underline{Z}} \tag{3.40}$$

But since $\sin 2\theta = 2\sin\theta \cos\theta$ and $\sin 4\theta = 4\sin\theta \cos\theta \cos 2\theta$ then

$$\frac{\partial b}{\partial \underline{Z}} = (4c_2 \cos\theta + 16c_3 \cos\theta \cos 2\theta) \hat{\underline{u}}^T \frac{\partial \hat{\underline{R}}}{\partial \underline{Z}} \tag{3.41}$$

If $\hat{\underline{R}}$ is given in equinoctial coordinates where $\hat{\underline{R}} = (X_s, Y_s, Z_s)$ then the nonzero partials are given by

$$\frac{\partial X_s}{\partial p} = \frac{-2}{1 + p^2 + q^2} (qY_s + Z_s) \tag{3.42}$$

$$\frac{\partial X_s}{\partial q} = \frac{2pY_s}{1 + p^2 + q^2} \tag{3.43}$$

$$\frac{\partial Y_s}{\partial p} = \frac{2qX_s}{1 + p^2 + q^2} \tag{3.44}$$

$$\frac{\partial Y_s}{\partial q} = \frac{2}{1 + p^2 + q^2} (-pX_s + Z_s) \tag{3.45}$$

$$\frac{\partial Z_s}{\partial p} = \frac{2X_s}{1 + p^2 + q^2} \tag{3.46}$$

$$\frac{\partial Z_s}{\partial q} = \frac{-2Y_s}{1 + p^2 + q^2} \tag{3.47}$$

The control must maximize the Hamiltonian. That portion of the unaveraged Hamiltonian containing the control is

$$H' = b(\hat{\underline{u}})\ \underline{\lambda}^T M\ \hat{\underline{u}} \tag{3.48}$$

Now b is considered a function of $\hat{\underline{u}}$ rather than θ. It is convenient to identify the primer vector as

$$\underline{\lambda}_v = M^T \underline{\lambda} \tag{3.49}$$

and define the primer vector cone angle β where

$$\cos\beta = \hat{\underline{R}}^T\ \hat{\underline{\lambda}}_v \tag{3.50}$$

The Hamiltonian is then

$$H' = b(\hat{\underline{u}})\ \underline{\lambda}_v^T\ \hat{\underline{u}} \tag{3.51}$$

The control $\hat{\underline{u}}$ can be written as a function of two angles, the cone angle θ and a clock angle, ψ. Then

$$\hat{\underline{u}} = (\cos\psi\ \hat{\underline{e}}_1 + \sin\psi\ \hat{\underline{e}}_2)\ \sin\theta + \cos\theta\ \hat{\underline{e}}_3 \tag{3.52}$$

where the unit vectors are given by

$$\hat{\underline{e}}_3 = \hat{\underline{R}} \tag{3.53}$$

$$\hat{\underline{e}}_2 = \underline{e}_3 \times \underline{V} \tag{3.54}$$

$$\hat{\underline{e}}_1 = \hat{\underline{e}}_2 \times \hat{\underline{e}}_3 \tag{3.55}$$

where $\underline{V}$ is a reference vector. In this coordinate frame the primer vector can be given in terms of β and a clock angle ψ_p. Then

$$\hat{\underline{\lambda}}_V = (\cos\psi_p\ \hat{\underline{e}}_1 + \sin\psi_p\ \hat{\underline{e}}_2)\ \sin\beta + \cos\beta\ \hat{\underline{e}}_3 \qquad (3.56)$$

The relevant portion of the Hamiltonian is then

$$H' = b(\theta)(\cos\psi\ \cos\psi_p + \sin\psi\ \sin\psi_p)\ \sin\theta\ \sin\beta + \cos\theta\ \cos\beta \qquad (3.57)$$

Maximizing H' with respect to θ and ψ is equivalent to maximizing H' with respect to $\hat{\underline{u}}$. The clock angle for $\hat{\underline{u}}$ must be equal to the clock angle of the primer vector: $\psi = \psi_p$. Thus $\hat{\underline{R}}$, $\hat{\underline{\lambda}}_V$, and $\hat{\underline{u}}$ are in the same plane and from geometry:

$$\hat{\underline{u}} = \frac{\sin(\beta - \theta)}{\sin\beta}\ \hat{\underline{R}} + \frac{\sin\theta}{\sin\beta}\ \hat{\underline{\lambda}}_V \qquad (3.58)$$

(as in Ref. 6).

The H' reduces to

$$H' = (c_1 + c_2\cos2\theta + c_3\cos4\theta)(\cos\theta\ \cos\beta + \sin\theta\ \sin\beta) \qquad (3.59)$$

This can be maximized with respect to θ by setting its derivative with respect to θ to zero.

$$\frac{\partial H}{\partial\theta} = (-2c_2\ \sin2\theta - 4c_3\ \sin\ 4\theta)(\cos\theta\ \cos\beta + \sin\theta\ \sin\beta)$$

$$+ (c_1 + c_2\ \cos2\theta + c_3\ \cos\ 4\theta)(-\ \sin\theta\ \sin\beta + \cos\theta\ \sin\beta)$$

$$= 0 \qquad (3.60)$$

Now for the idealized flat square sail $c_1 = c_2 = 0.5$ and $c_3 = 0$ so that $b(\theta) = \cos^2\theta$. Then $\frac{\partial H}{\partial\theta} = 0$ can be reduced to a quadratic in $\tan\theta$ whose solution is

$$\tan\theta = \frac{-\ 3\cos\beta + \sqrt{8\sin^2\beta + 9\cos^2\beta}}{4\sin\beta} \qquad (3.61)$$

where note that β can vary between 0 and 180°, but θ varies between 0 and 90°. This is similar to Ref. 6. In the general case, the expression could be reduced to a polynomial, but it is easier to solve the equation numerically using a Newton method. If

$$H = b(\theta)\, d(\theta) \tag{3.62}$$

where

$$d(\theta) = \cos\theta \cos\beta + \sin\theta \sin\beta \tag{3.63}$$

let

$$f(\theta) = \frac{\partial H}{\partial \theta} = b'(\theta)\, d(\theta) + b(\theta)\, d'(\theta) \tag{3.64}$$

The prime indicates the derivative with respect to θ. An initial guess for θ is given by the solution for the idealized sail, Eq. (3.61). Then iterate

$$\theta_{n+1} = \theta_n - \frac{f_n}{f'_n} \tag{3.65}$$

Until $\theta_{n+1} - \theta_n < c$, some small positive number. Also needed is

$$f' = \frac{\partial f}{\partial \theta} = 2b'd' + b''d + bd'' \tag{3.66}$$

where

$$b'' = -4c_2 \cos 2\theta - 16c_3 \cos 4\theta \tag{3.67}$$

and

$$d'' = -d \tag{3.68}$$

Thus the control $\hat{u}$ is determined.

Figure 3-4 shows the variation of θ with β for the idealized sail and for one set of coefficients: $c_1 = 0.367$, $c_2 = 0.643$, $c_3 = -0.010$ which corresponds to one, JPL supplied, heliogyro model. Note the cut off angle of $\theta = 62.6°$ which occurs in a region where the model is not realistic. In the computer program, whenever the optimization

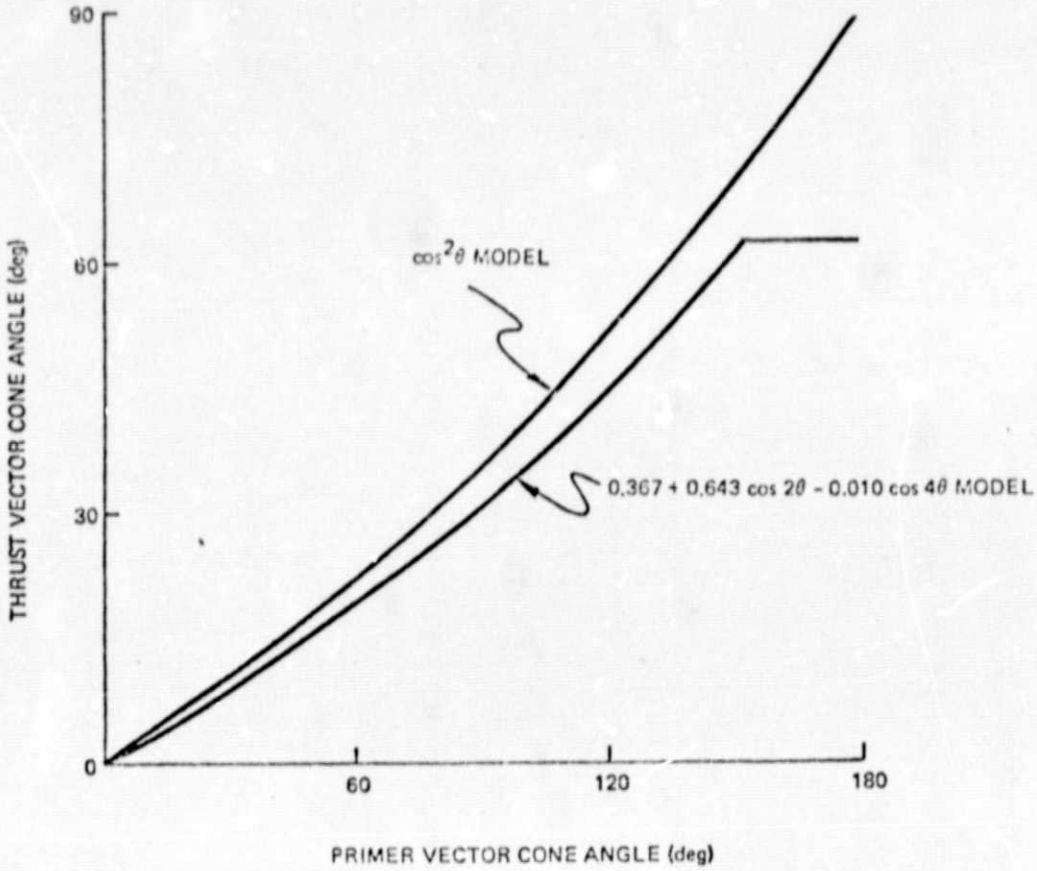

Figure 3-4. Thrust vector cone angle versus primer vector cone angle.

called for a θ greater than this cutoff value, θ was set to the cutoff value as indicated in the figure. The cutoff angle was given by Eq. (3.7).

The state and costate differential equations have been given and the optimal control derived. It remains to specify the transversality conditions. For transfer to a subescape point, the final energy, or equivalently, the final semimajor axis is specified.

$$E = \frac{m}{2} C_3 = -\frac{m}{2} \frac{\mu}{a} \tag{3.69}$$

This is equivalent to specifying the final semimajor axis since the mass, m, is constant. Transversality conditions then require that the adjoints to the remaining state variables be zero and that the Hamiltonian be equal to one at the final time.

$$\lambda_h = 0$$
$$\lambda_k = 0$$
$$\lambda_p = 0$$
$$\lambda_q = 0$$
$$H = \underline{\lambda}^T \dot{\underline{Z}} = 1 \qquad (3.70)$$

The adjoints to the classical orbital elements, e, i, Ω, and ω should also be zero at the final time.

In the case of orbit transfer, if the orbit is completely specified (a, e, i, Ω, ω or equivalently a, h, k, p, q) at the final time, then their adjoints are free and the only transversality condition is that the final Hamiltonian be one. If three orbital elements (the semimajor axis, eccentricity, and inclination) are specified at the final time, then the Hamiltonian must be one and λ_Ω and λ_ω must be zero. In terms of equinoctial elements and their adjoints the following final state conditions are specified:

$$a = a(t_f)$$
$$\sqrt{h^2 + k^2} = e(t_f) \qquad (3.71)$$
$$\sqrt{p^2 + q^2} = \tan(i(t_f)/2)$$

The transversality conditions are:

$$h\lambda_k - k\lambda_h = \lambda_\omega(t_f) = 0$$
$$p\lambda_q - q\lambda_p = \lambda_\Omega(t_f) = 0 \qquad (3.72)$$
$$H = 1$$

The state and costate differential equations and the initial and final conditions yield a two-point boundary-value problem. This problem can be solved with an iterative method. A Newton method was used as in Ref. 12. The differential equations were integrated numerically with a Runge-Kutta method. At each function evaluation for the Runge-Kutta method a numerical quadrature was used to average the equations (3.33) and (3.34). The control was found using Eq. (3.58) and by a Newton search

for the cone angle. Additional complexity is added by including a penality function, shadowing and oblateness.

3.4 Pericenter Penalty Function

Planetocentric solar sail trajectories typically build up large eccentricity rapidly. This can be particularly undesirable if the initial altitude is low. Optimization may actually yield trajectories that intersect the planet's surface. Also, large eccentricity orbits often require rapid changes in thrust direction which, in practice, may be impossible to implement. One way of reducing this problem is to append a penalty function to the cost (which has been flight time). One possible penalty is the integral over the flight time of the inverse pericenter squared. Then the cost is given by

$$J = t_f + \frac{\eta}{2} \int_{t_0}^{t} \frac{1}{r_p^2} \, dt \tag{3.73}$$

This penalizes low altitudes in general and especially at small semimajor axis. To some extent it also penalizes larger eccentricities. The constant, η, must be picked to obtain a desirable weighting between the penalty and the flight time. Experience with a few example cases indicated that this method could be used to prevent altitudes which were too small with a very small increase in flight time (less than 5%). Other penalty functions might be used, for example, one which is much steeper near some specific altitude, thus acting as an inequality constraint (see Ref. 25).

The Hamiltonian and the costate equations must be modified. The pericenter is given in equinoctial elements by

$$r_p = \frac{1}{a(1 - \sqrt{h^2 + k^2})} \tag{3.74}$$

If

$$L = \frac{\eta}{2} \frac{1}{a^2(1 - \sqrt{h^2 + k^2})^2} \tag{3.75}$$

then the Hamiltonian is given by

$$H = \underline{\lambda}^T \dot{\underline{Z}} - L \tag{3.76}$$

The averaged Hamiltonian is

$$\tilde{H} = \frac{1}{T_o} \int_0^{T_o} \underline{\lambda}^T \dot{\underline{Z}} \, dt + \frac{1}{T_o} \int_0^{T_o} L(\underline{Z}) \, dt \tag{3.77}$$

and the costate equation is

$$\dot{\underline{\lambda}}^T = - \frac{\partial H}{\partial \underline{Z}} \tag{3.78}$$

The first integral in Eq. (3.77) is the same as if there were no penalty function. The second integral does not include a time dependence in the integrand and so it is just equal to $L(\underline{Z})$. Thus, the only thing different in Eq. (3.78) is the addition of $\frac{\partial L}{\partial \underline{Z}}$. In particular

$$\frac{\partial L}{\partial a} = - \frac{2L}{a} \tag{3.79}$$

$$\frac{\partial L}{\partial h} = - \frac{2L}{1 - \sqrt{h^2 + k^2}} \frac{h}{\sqrt{h^2 + k^2}} \tag{3.80}$$

$$\frac{\partial L}{\partial k} = \frac{2L}{1 - \sqrt{h^2 + k^2}} \frac{k}{\sqrt{h^2 + k^2}} \tag{3.81}$$

$$\frac{\partial L}{\partial p} = \frac{\partial L}{\partial q} = 0 \tag{3.82}$$

Transversality conditions still require that the final Hamiltonian be equal to one, but in this case at t_f:

$$H = \underline{\lambda}^T \dot{\underline{Z}} - L = 1 \tag{3.83}$$

3.5 Oblateness

In the previous sections we have considered only perturbations to the inverse square motion caused by thrusting. In this section, the effect of oblateness (J_2) is considered. Oblateness equations are included here for convenience from Ref. 12. Oblateness is included only for earth-centered trajectories.

The single-averaged perturbing potential due to J_2 has been calculated in terms of equinoctial coordinates in Ref. 14 and is repeated in Appendix C. R_e is the equatorial radius of the Earth and J_2 is set to .001827. These formulas enter the averaged Hamiltonian as coefficients of the costate (outside the integral since the averaging effect has already been accounted for).

If $\dot{\underline{Z}}_a$ indicates the perturbation due to thrust as given in Eq. (3.33) then the Hamiltonian is given by

$$\tilde{H} = \underline{\lambda}^T \dot{\underline{Z}}_{J_2} + \underline{\lambda}^T \dot{\underline{Z}}_a \tag{3.84}$$

The state equation is

$$\dot{\underline{Z}} = \dot{\underline{Z}}_{J_2} + \dot{\underline{Z}}_a \tag{3.85}$$

The costate equation is

$$\dot{\underline{\lambda}}^T = -\frac{\partial \tilde{H}}{\partial \underline{Z}} = -\underline{\lambda}^T \frac{\partial \dot{\underline{Z}}_{J_2}}{\partial \underline{Z}} - \int_{-\pi}^{\pi} \left[\underline{\lambda}^T \frac{\partial \dot{\underline{Z}}_a}{\partial \underline{Z}} s + \underline{\lambda}^T \dot{\underline{Z}}_a \frac{\partial s}{\partial \underline{Z}} \right] dF \tag{3.86}$$

The partials indicated by $\partial \dot{\underline{Z}}_{J_2} / \partial \underline{Z}$ in the above expression are given in Appendix C.

3.6 The Shadow Effect

For solar sail missions, there is no thrust while the spacecraft is in a planet's shadow. The entry and exit angles are needed in order to perform the averaging integral. In calculating these angles the following assumptions are made. The shadow is cylindrical; the planet revolves around the sun in an elliptical orbit; and over one spacecraft revolution, the sun's direction is fixed. Pertinent equations for the calculation of the entry and exit eccentric longitudes are summarized in Appendix D taken from Ref. 12.

Let F_2 refer to the eccentric longitude at entry to the shadow and F_1 at exit. That part of the Hamiltonian proportional to thrust is then

$$\tilde{H} = \int_{F_1}^{F_2} H\, s\, dF \tag{3.87}$$

Thus

$$\dot{\underline{Z}} = \int_{F_1}^{F_2} \dot{\underline{Z}}\, s\, dF \tag{3.88}$$

and by Leibnitz' rule

$$\dot{\underline{\lambda}} = -\int_{F_1}^{F_2} \left(\frac{\partial H}{\partial \underline{Z}}\, s + H\, \frac{\partial s}{\partial \underline{Z}} \right) dF - \left[\frac{dF}{d\underline{Z}}\, Hs \right]_{F_2} + \left[\frac{dF}{d\underline{Z}}\, Hs \right]_{F_1} \tag{3.89}$$

The calculation of $\frac{dF}{d\underline{Z}}$ is discussed in Appendix D.

3.7 Planetary Data and Coordinate Frames

Earlier versions of the code for electric propulsion trajectories assumed Earth orbital missions with spacecraft orbital elements referenced to an equatorial coordinate frame. The solar sail program has been generalized to include trajectories about the four inner solar system planets: Mercury, Venus, Earth, and Mars. The gravitational constant for each planet is given in Table 3-1. Also given is the planet's radius. This is used in shadow calculations and also the "internal units" of the code use planetary radii. Oblateness, J_2, is assumed zero for all planets except Earth. The characteristic acceleration of a solar sail is defined as the maximum acceleration at 1 A.U. Thus, the planet's distance from the sun is needed as well as the sun's direction. An equatorial coordinate frame is used only for Earth trajectories. The obliquity angle, the angle between the Earth's equator and the ecliptic, is thus needed. For all the planets an ecliptic frame may be used. In this frame the X- and Y-axes are in the ecliptic with

the X-axis toward the vernal equinox direction and the Z-axis is normal to the ecliptic in a "northerly" direction. Another coordinate frame option is the "planetary" frame which is referenced to the planet's orbital plane, the Z-axis normal to the orbital plane, the X-axis pointed toward perihelion.

Table 3-1. Planetary data.

	Mercury	Venus	Earth	Mars
Semimajor axis, a (A.U.)	0.387099	0.723322	1.0	1.523691
Eccentricity, e	0.205627	0.006793	0.016726	0.093368
Inclination, i (°)	7.00399	3.39423	0.	1.84991
Longitude of the ascending node, Ω(°)	47.85714	76.31972	0.	49.24903
Mean longitude of perihelion $\bar{\omega}$ (°)	76.83309	131.00831	102.25253	335.32269
Mean orbital motion, n (°/day)	4.092339	1.602131	0.985609	0.524033
Mean longitude at epoch, ϵ	222.62165	174.29431	100.15815	258.76729
Obliquity angle (°)	----	----	23.45	----
J_2	----	----	0.0010827	----
Radius (km)	2435.0	6052.0	6378.16	3393.4
Gravitational constant, μ (km^3s^{-2})	22181.6	324860.1	398601.2	42828.4

Data for Epoch 1960 Jan 1.5 E.T. (J.D. 2436935.0) from Ref. 26 except J_2, radius and μ from Ref. 27.

In the ecliptic coordinate frame the unit vector pointing from the planet toward the sun is

$$\hat{\underline{R}}_s = \begin{bmatrix} \cos\Omega & -\cos i\,\sin\Omega & \sin i\,\sin\Omega \\ \sin\Omega & \cos i\,\cos\Omega & -\sin i\,\cos\Omega \\ 0 & \sin i & \cos i \end{bmatrix} \begin{bmatrix} -\cos(v+\omega) \\ -\sin(v+\omega) \\ 0 \end{bmatrix} \quad (3.90)$$

Note that for Earth, i and Ω are zero so that the matrix is the identity matrix. The argument of perihelion ω is obtained from Table 3-1 since

$$\omega = \bar{\omega} - \Omega \tag{3.91}$$

The angle v is the true anomaly. It can be approximated by (Ref. 26)

$$v = M + \left(2e - \frac{e^3}{4}\right) \sin M + \frac{5}{4} e^2 \sin 2M + \frac{13}{12} e^3 \sin 3M \tag{3.92}$$

where M is the mean anomaly and

$$M = n\tau + M_o \tag{3.93}$$

The time τ is measured from the epoch and M_o is the mean anomaly at epoch:

$$M_o = \varepsilon - \bar{\omega} \tag{3.94}$$

The mean orbital motion, n, is given in the table with other needed constants.

The distance to the sun in A.U.'s is

$$|R_s| = \frac{a(1 - e^2)}{1 + e \cos v} \tag{3.95}$$

The difference between the sun-spacecraft distance and the sun-planet distance is assumed negligible.

For an Earth-equatorial frame

$$\hat{\underline{R}}'_s = \begin{bmatrix} -\cos(\omega+v) \\ -\cos O \sin(\omega+v) \\ -\sin O \cos(\omega+v) \end{bmatrix} \tag{3.96}$$

where O is the obliquity of the ecliptic.

For a "planetary" frame i, Ω, and ω in Eq. (3.90) are set to zero.

In the equinoctial coordinate frame

$$\hat{\underline{R}}_S = [\hat{\underline{f}}, \hat{\underline{g}}, \hat{\underline{w}}]^T \hat{\underline{R}}'_S \qquad (3.97)$$

where the equinoctial basis vectors were given in Eq. (3.11). Note that the $\underline{R}$ vector used in earlier equations in this section is the vector from the sun to the planet rather than from the planet to the sun.

SECTION 4

NUMERICAL RESULTS

A number of example runs were performed. A complete performance analysis was not done because of the continuing change in status of the solar sail mission planning. First the square sail was emphasized. Then the heliogyro was picked as the principal solar sail design. Finally, the solar sail lost in competition with ion drive as a contender for near future low thrust missions. A complete heliogyro model was not implemented. Results in this section are for the square sail model discussed in Section 3. A limited number of Earth-centered trajectories will be discussed here. Because of decreased interest, further runs were not performed. No trajectories about the other inner planets are included since the only cases that were run were short test cases to verify the coding. A test case also verified the use of the program to calculate trajectories which spiral down from a high near-capture orbit to a lower orbit. This is a special case of orbit transfer.

A number of cases using the square sail approximation with heliogyro coefficients (C_1 = 0.367; C_2 = 0.643; C_3 = -0.010) for transfer to a subescape point will be discussed. These runs used a 10 day time step and four 4-point gaussian quadratures for the averaging integral. A subescape point with a semimajor axis of 100,000 or 200,000 km was used (this is equivalent to a C_3 of -3.99 or -1.99 km^2/s^2, respectively). A number of factors determine flight time. The initial orbit is, of course, of critical importance. An initial orbit with a semimajor axis of 21378 km, eccentricity of 0.655 was suggested by JPL personnel. This initial orbit would be representative of a tug-launched sail (C_3 = -18.6 km^2/s^2). The longitude of the ascending node (Ω) and the argument of perigee (ω) can be varied. The inclination (i) can be varied but differing launch energies would be required if the launch day is fixed. A number of open loop trajectories were run to get a feeling for the i, Ω, and ω that would yield the lower flight times. Then trajectories were optimized for a few cases of specific i, Ω, and

ω (for convenience, these angles were specified with respect to an ecliptic frame). A launch of March 21, 1984 was assumed. Although an elliptical Earth orbit about the sun was modeled, the $1/R^2$ effect of solar pressure was not included in the examples (a constant 1 A.U. distance was assumed). Earlier examples indicated that including oblateness has a very small effect on flight times and therefore this effect was not included in the examples shown here. Shadowing was included but the initial orbits were chosen to avoid the shadowed regions.

The results for seven examples are shown in Table 4-1. Cases 1, 3, and 4 show the effect of varying characteristic acceleration from 0.6 to 1.0 mm/s^2. These cases are also plotted in Fig. 4-1. Case 2 has a final semimajor axis of 200,000 km rather than 100,000 km as in Case 1. An additional 20 days is needed. At 100,000 km the orbital period is 3.6 days and at 200,000 km it is 10.3 days. Escape would probably occur in less than 30 more days, about two more revolutions. Apocenter for the final orbit was at 347,000 km where the thrust/weight ratio was nearly 0.1 for the 0.6 mm/s^2 acceleration, so that the averaging technique has limited validity there.

Case 5 is similar to Case 1 except that the initial orbit is circular rather than elliptical. The initial C_3 for both cases is -18.6 km^2/s^2. The transfer time to a C_3 of -3.99 is about 4 days longer for the initially circular orbit case. This behavior is due to the fact that the initial orientation of the elliptical orbit was chosen so that the sail was moving away from the sun near apocenter. At this point, the sail was moving more slowly and therefore, received more energy. Thus, for the first 80 days of Case 1, the eccentricity actually decreases to below 0.2.

Cases 6 and 7 have initial orbits which are normal to the ecliptic and chosen so that as the Earth moves around the sun, the orbits will come closer to being normal to the sunline. Slightly increased transfer times resulted compared to the 45° inclination cases. For Case 6, the eccentricity became smaller and at the final time was equal to .004. The initial costates are shown for all the runs.

Case 1 will be illustrated in more detail by a series of figures. Figures 4-2 to 4-6 are plots of the classical orbital elements (a, e, i, Ω, and ω). Since the initial time is March 21, the x-axis of the coordinate frame is pointing toward the sun at the initial time. Eccentricity and inclination decrease for the first 80 days. The line

TABLE 4-1

Transfer to a Subescape Point

CASE	1	2	3	4	5	6	7
Initial a (km)	21378	21378	21378	21378	21378	21378	21378
e	0.655	0.655	0.655	0.655	0.0	0.655	0.655
i	45°	45°	45°	45°	45°	90°	90°
Ω	150°	150°	150°	150°	150°	0°	0°
ω	180°	180°	180°	180°	180°	-90°	-90°
Characteristic Acceleration (mm/s^2)	0.6	0.6	0.8	1.0	0.6	0.6	0.6
Final a (km)	100000	200000	100000	100000	100000	100000	200000
Flight Time (days)	116.5	147.4	88.1	70.9	120.3	122.8	153.3
Costate λ_a	3389	3750	2579	2097	3444	3753	3653
λ_r	256	84	-112	-249	-801	1272	1616
λ_k	-458	-464	-366	-347	1365	66	66
λ_p	-869	-2614	-966	-972	-603	763	804
λ_q	1840	920	1312	977	1059	-2	-1

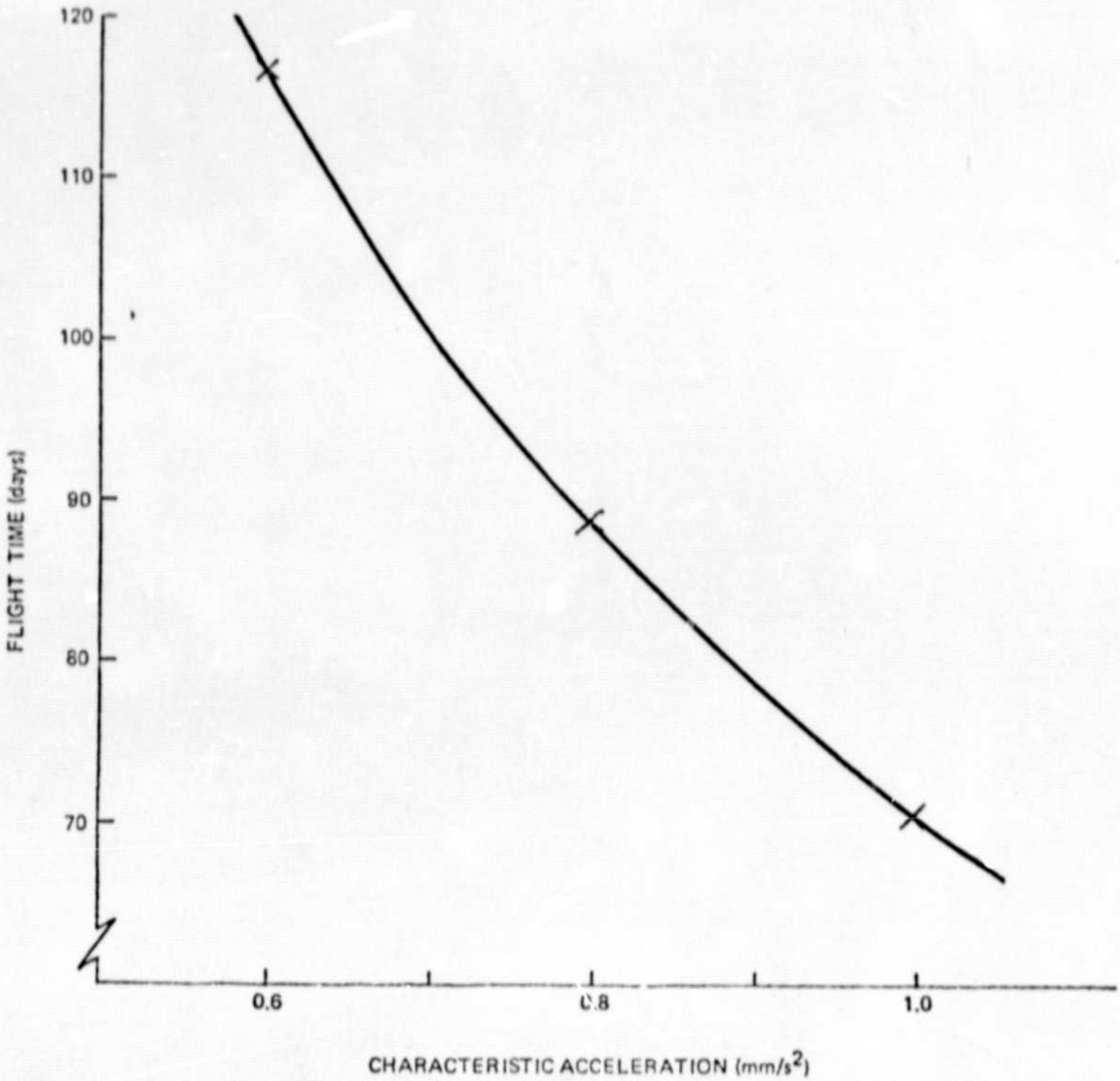

Figure 4-1 Flight time versus characteristic acceleration

Figure 4-2 Semimajor axis history

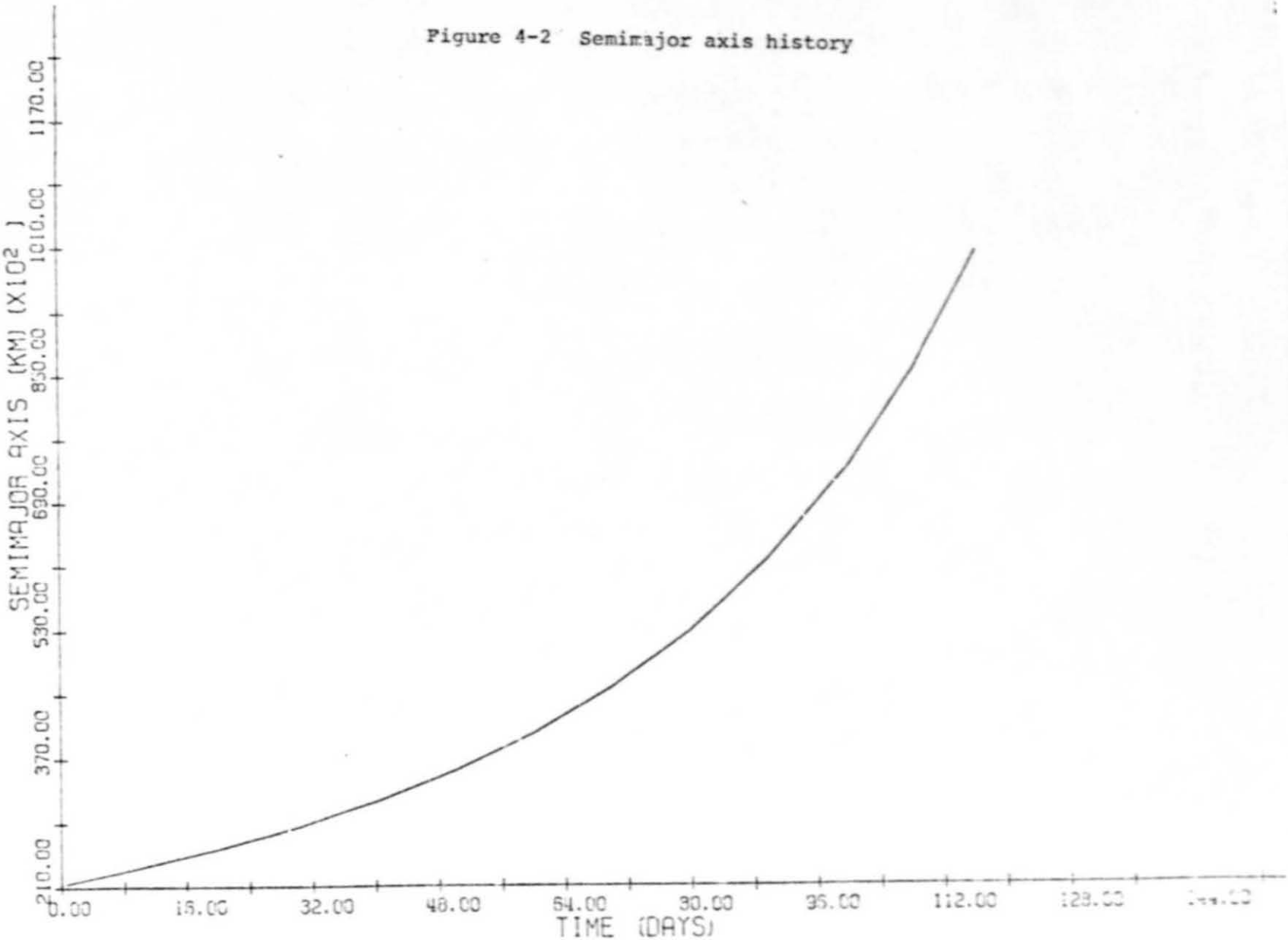

Figure 4-3 Eccentricity history

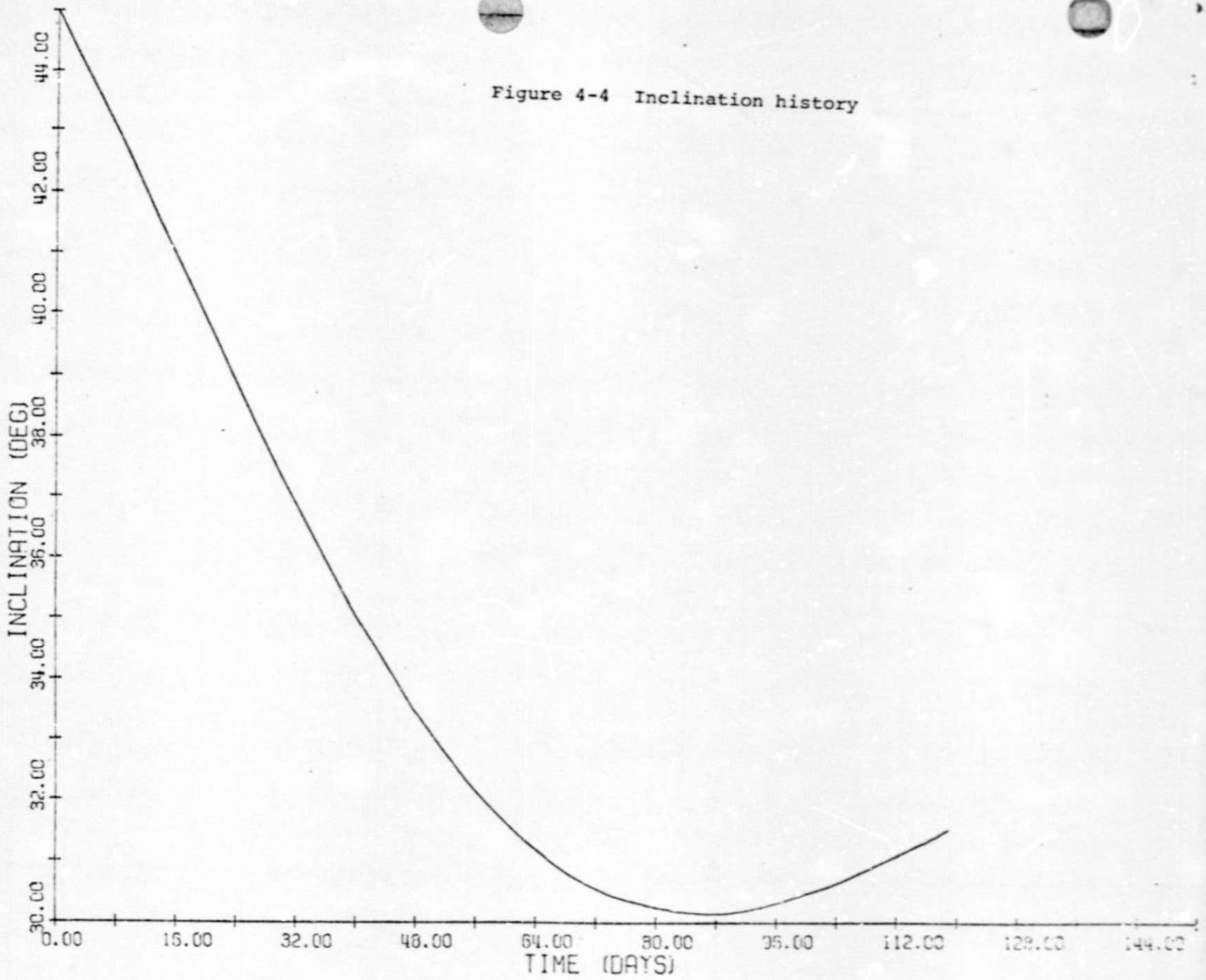

Figure 4-4 Inclination history

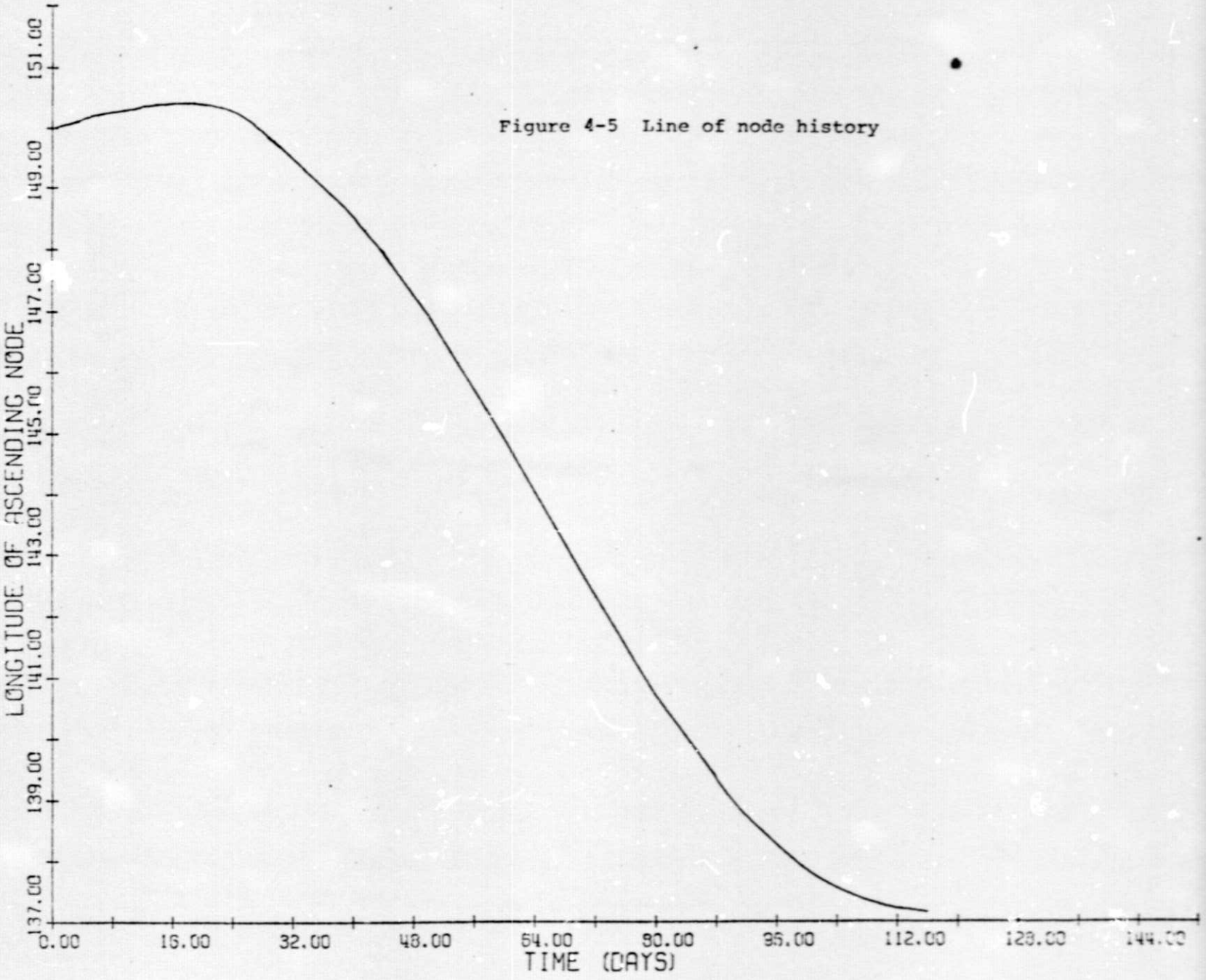

Figure 4-5 Line of node history

Figure 4-6 Argument of pericenter history

of nodes changes slightly but the argument of perigee increases from -180° to 35°. Figure 4-7 shows a plot of C_3. The dotted line at $C_3 = 0$ is the escape energy. Although shadowing was included, the trajectory never intersected the shadow. Fairly large changes in sail direction were required in a short time for early orbits. For example, on the first orbit a change in the sail direction of over 40° in 20 minutes was called for. This occurs in the region where the sail is near to edge-on with the sunline and the thrust produced is very small. In practice a slower non-optimal change in direction would probably have only a small effect on performance. The cone angle for the primor vector and the cone and clock angle for the thrust vector are shown in Figs. 4-8 to 4-10 for 3 orbits including the initial orbit, an orbit at 50 days, and the final orbit.

Figures 4-11 to 4-20 show the history of the equinoctial orbital elements and their adjoints for Case 1. The initial costate is shown in Table 4-1. When oblateness was included for the same initial conditions, the flight time was 116.42 days rather than 116.52 days. The corresponding costate is (3355, 227, -387, -698, 1877). A run with a five day time-step was not appreciably different than the ten-day case. The curves in Figs. 4-21 to 4-23 have not been smoothed; the ten day time step produces corners in the computer plot. Figures 4-21 to 4-23 illustrates the change in period, pericenter and apocenter.

Convergence characteristics for the cases of transfer to a sub-escape point were good. Typically an initial guess of $\lambda_a = 1000$ with the other adjoints zero resulted in convergence (to within 3 or 4 significant figures in the desired semimajor axis) in 4 or 5 iterations. This requires about 1 minute of CPU time on Draper Lab's Amdahl 470 (a fairly fast computer) at a cost of about $20.

An idealized sail was assumed for an orbit raising case ($c_1 = c_2 = 0.5$, $c_3 = 0$). A launch time of March 21, 1977 for an initial circular orbit with $a = 7878$ km, $i = 28.3^{\circ}$, $\Omega = 0^{\circ}$, $\omega = 0^{\circ}$ in an equatorial coordinate frame and with a characteristic acceleration of 1.0 mm/s^2 was specified. Shadowing was not included. The desired final orbit was equatorial geosynchronous. For this case the minimum transfer time was 195.8 days. The eccentricity increased to over 0.83 at 120 days before decreasing to zero. Unfortunately, the pericenter de-

Figure 4-7 C_3 history

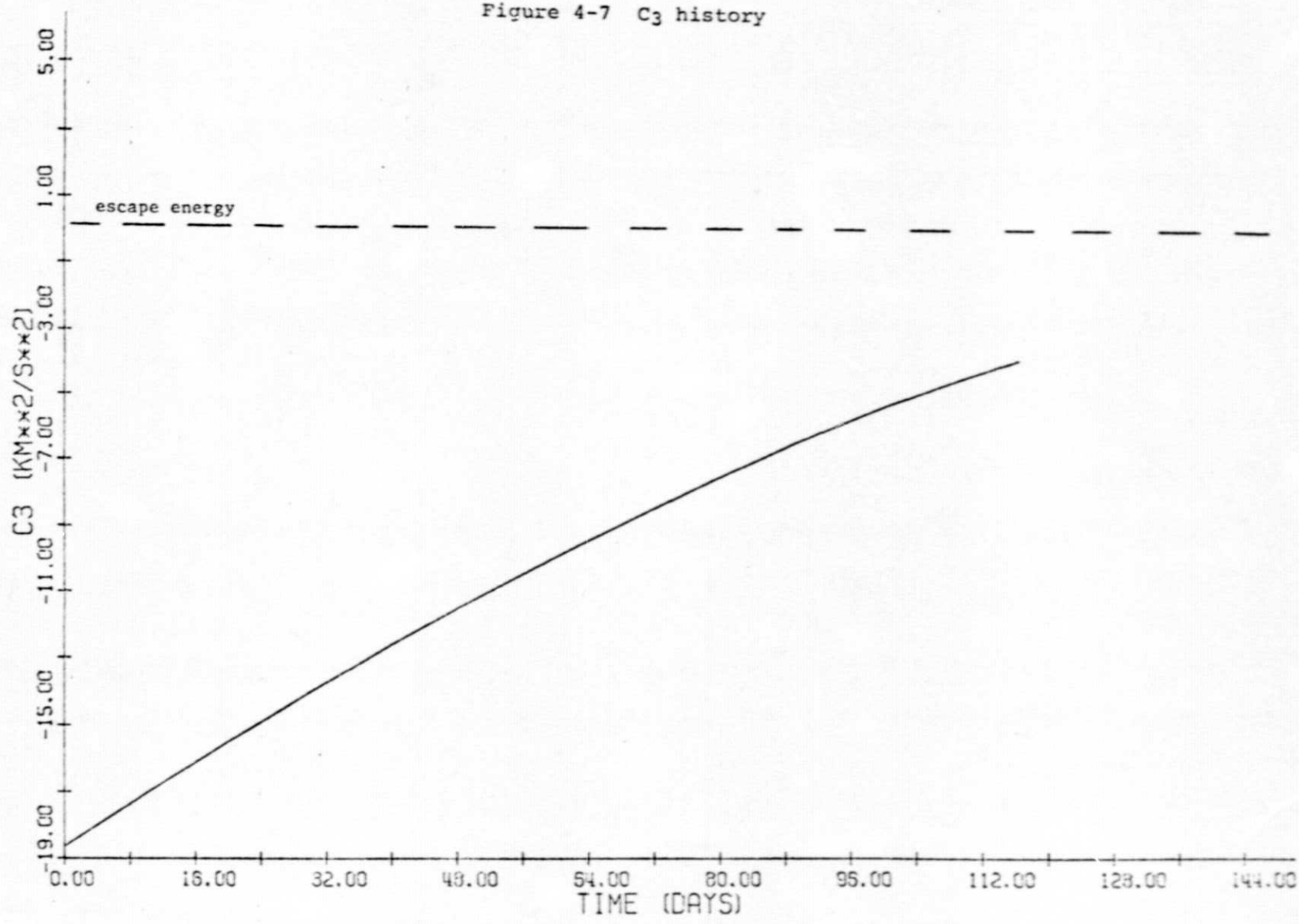

Figure 4-8 Primer and thrust angles

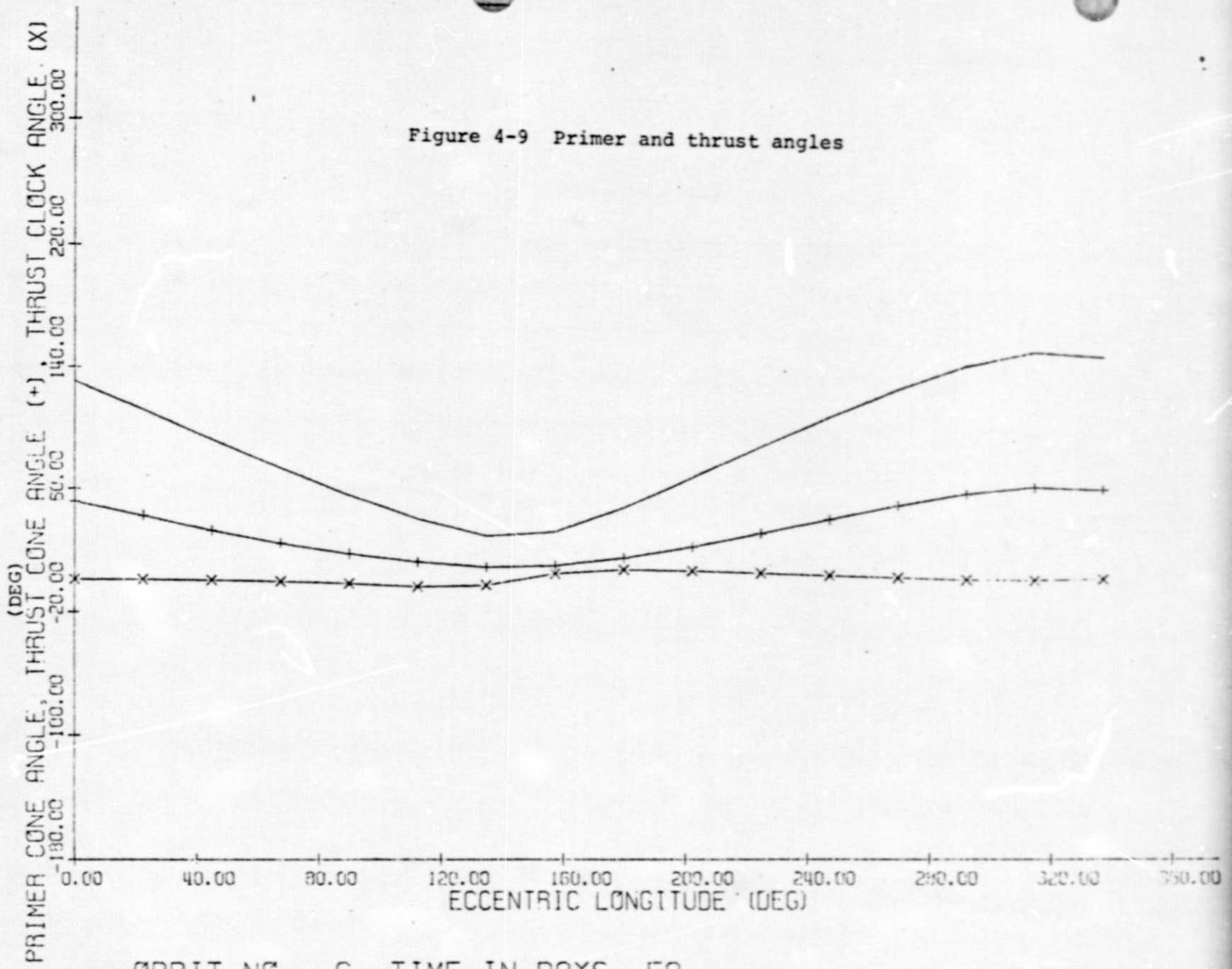

Figure 4-9 Primer and thrust angles

Figure 4-10 Primer and thrust angles

ORBIT NO.= 13, TIME IN DAYS= 116.52

Figure 4-11 Semimajor axis history in planetary radii

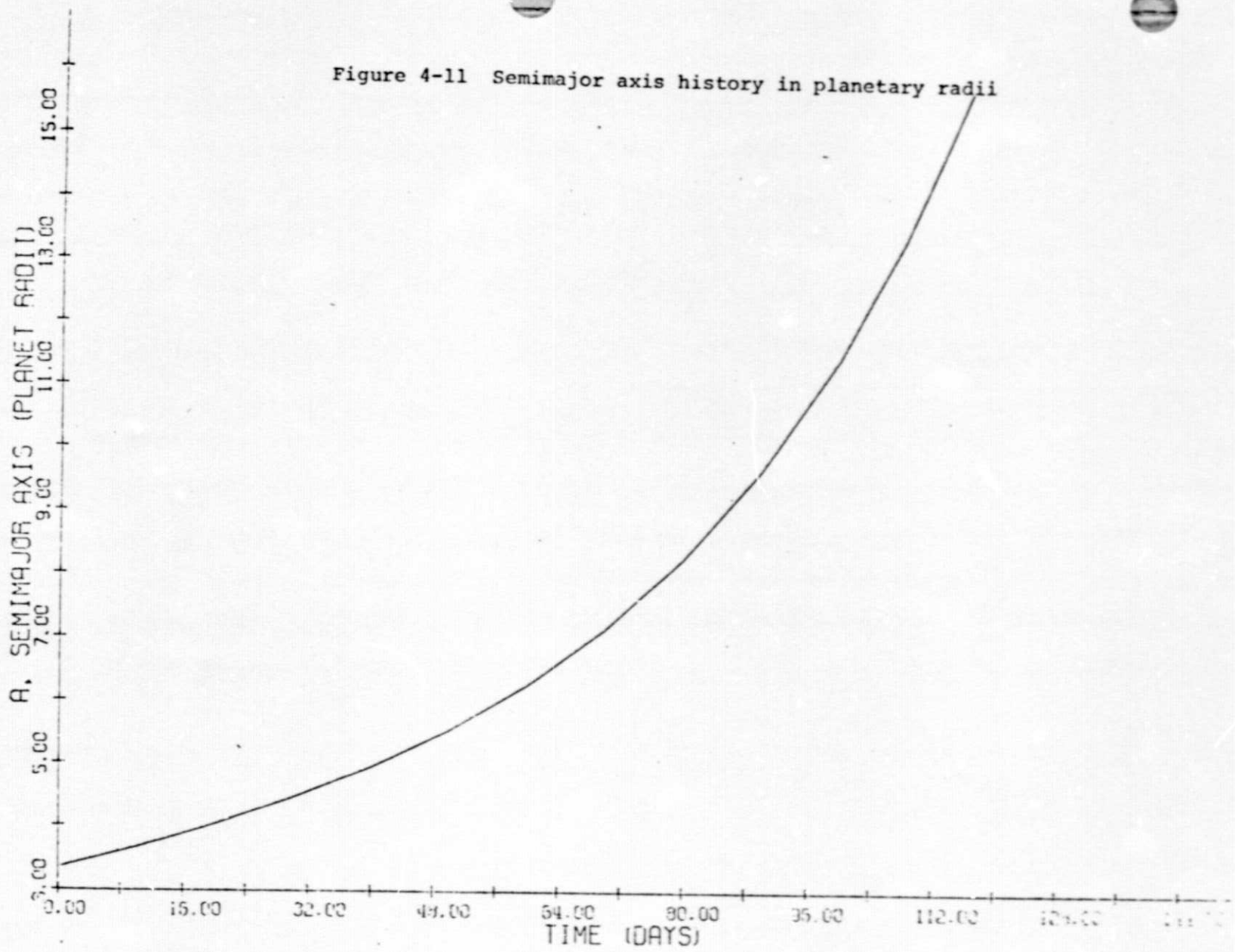

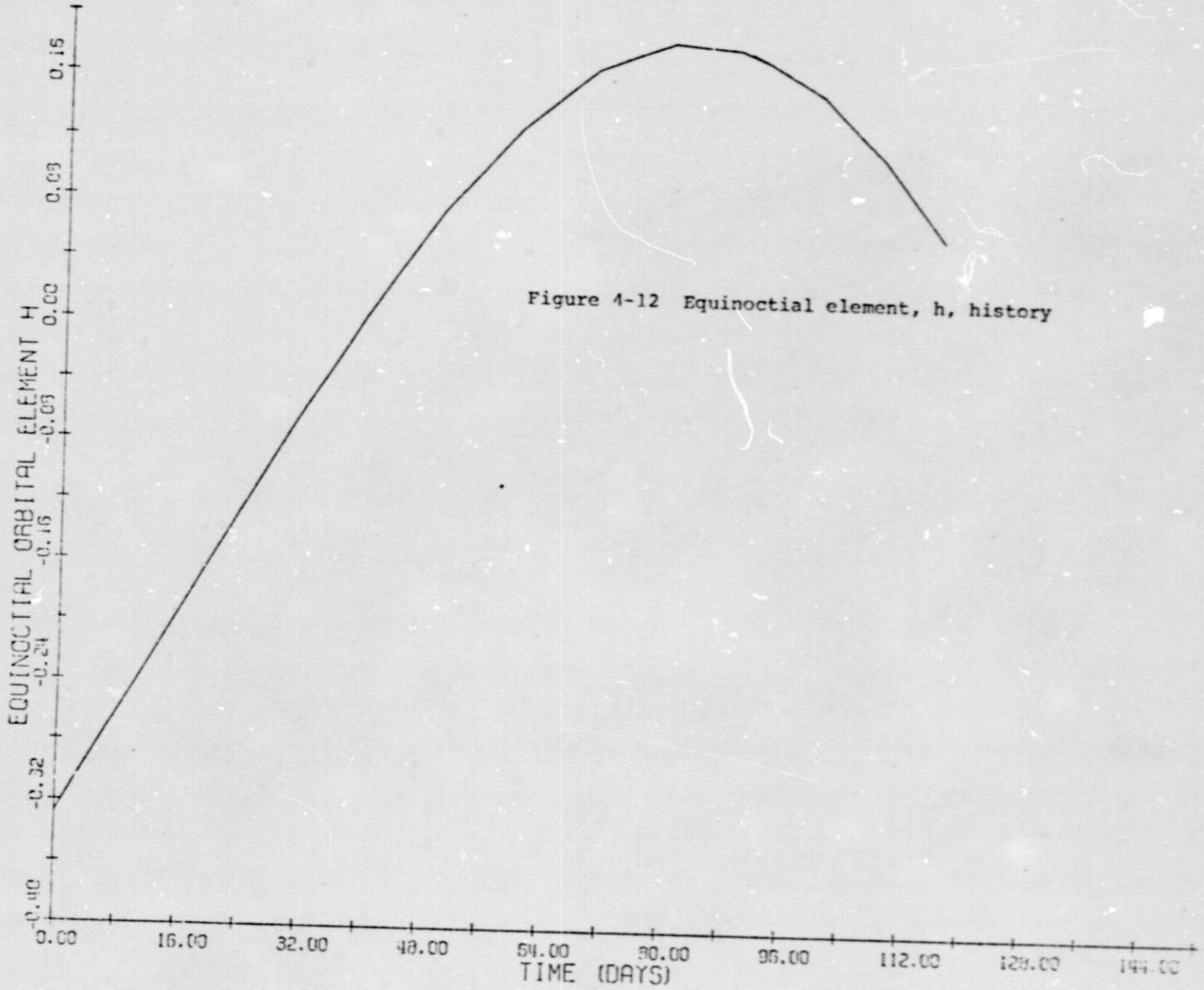

Figure 4-12 Equinoctial element, h, history

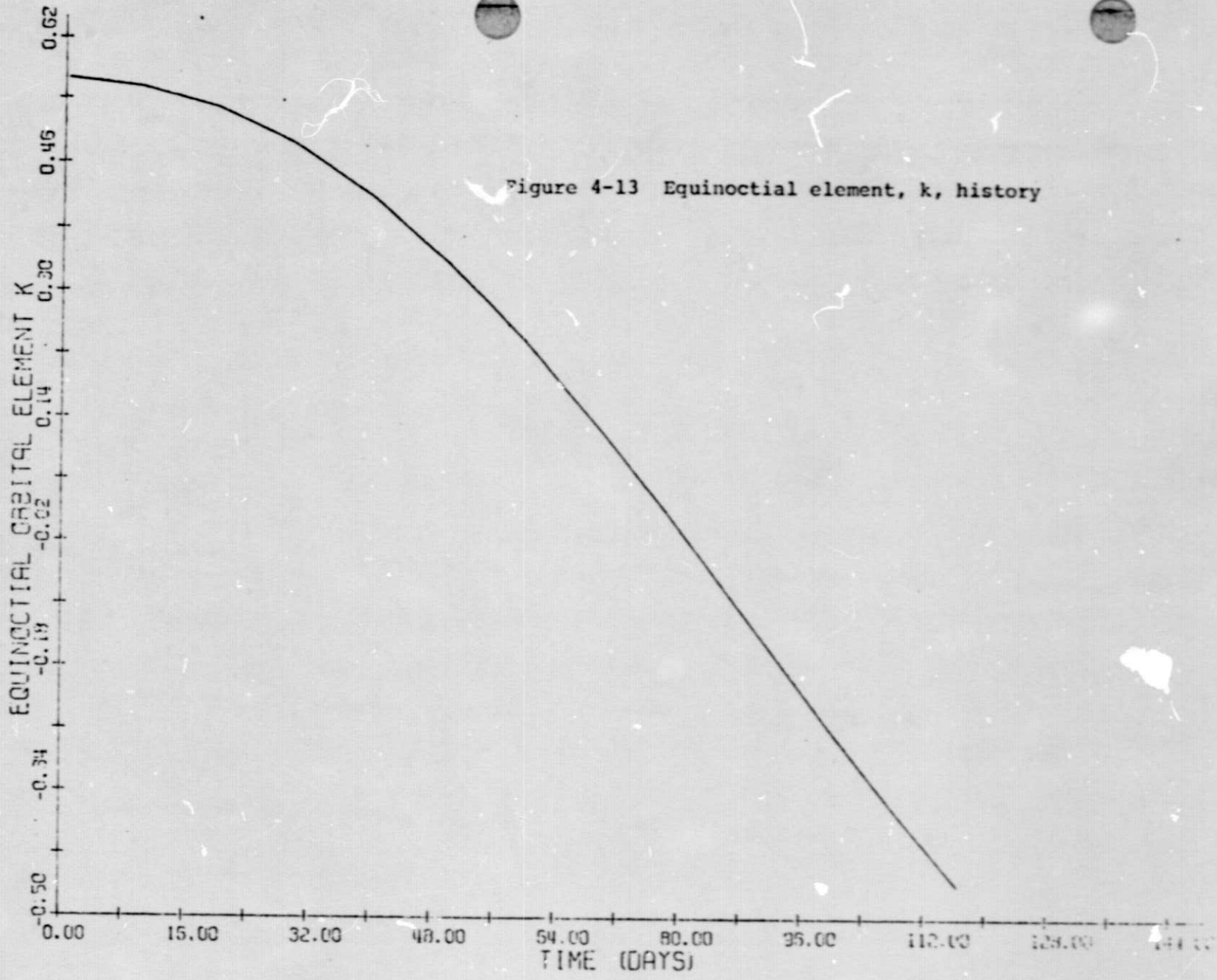

Figure 4-13 Equinoctial element, k, history

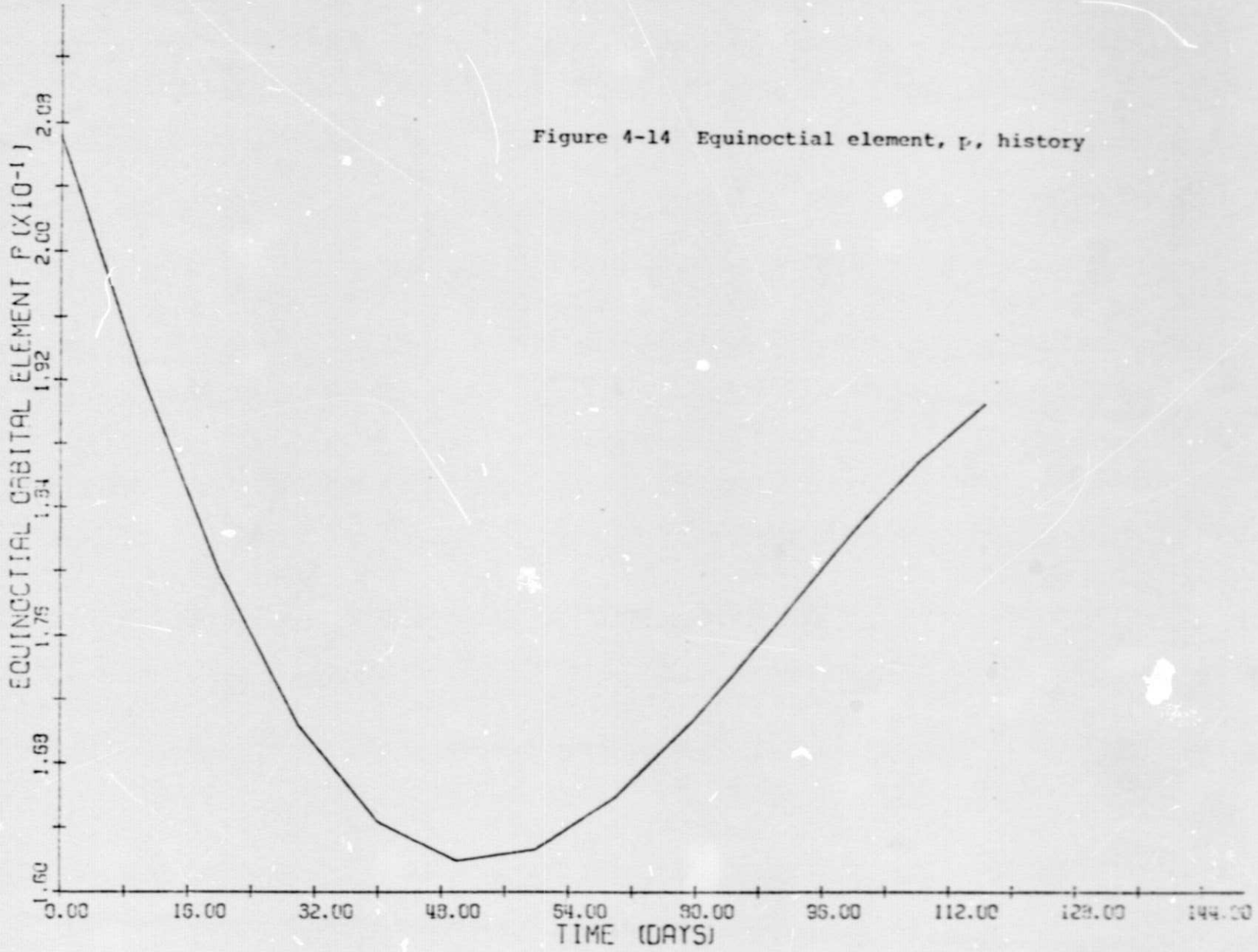

Figure 4-14 Equinoctial element, p, history

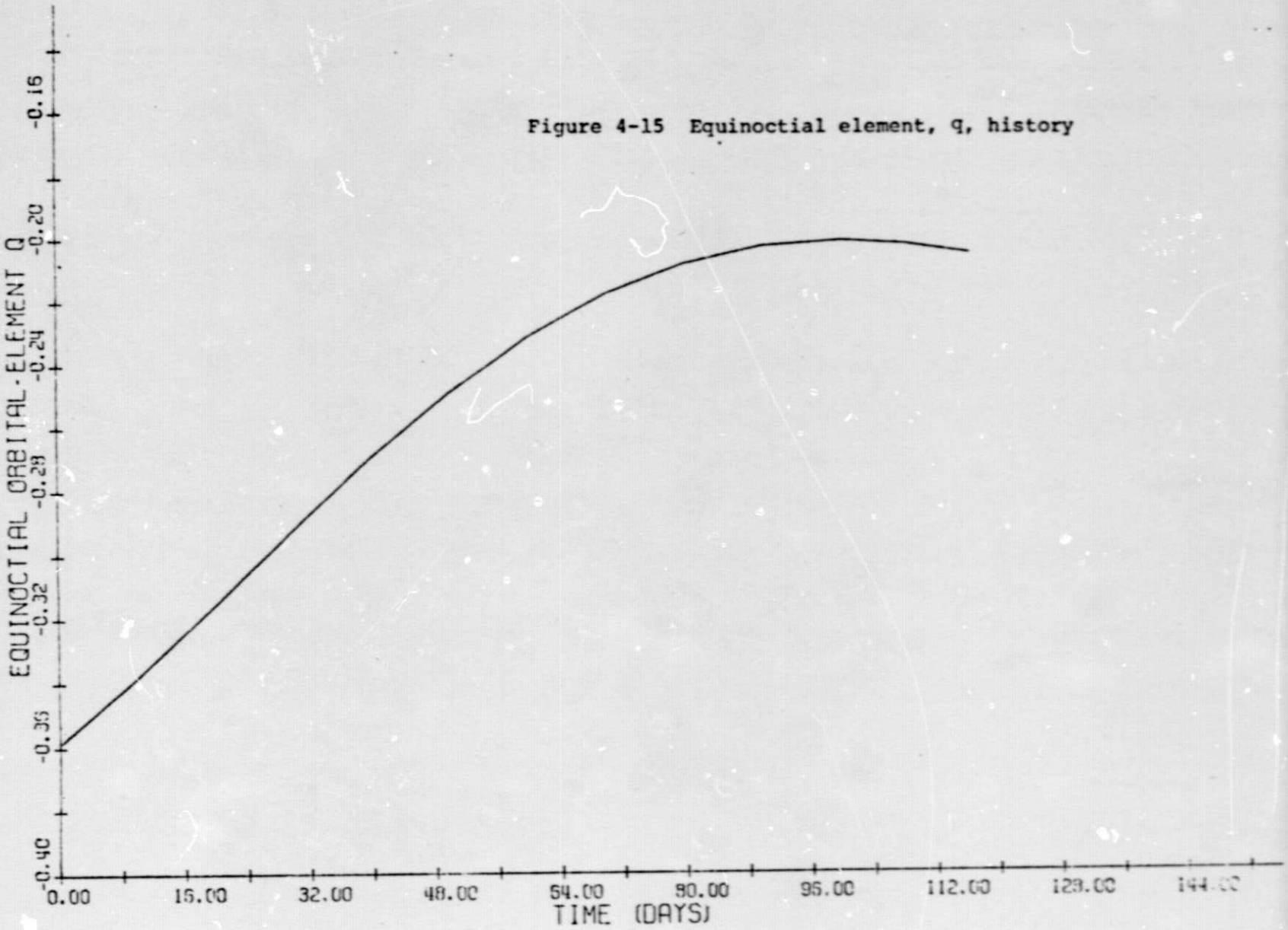

Figure 4-15 Equinoctial element, q, history

Figure 4-16 Costate, λ_a, history

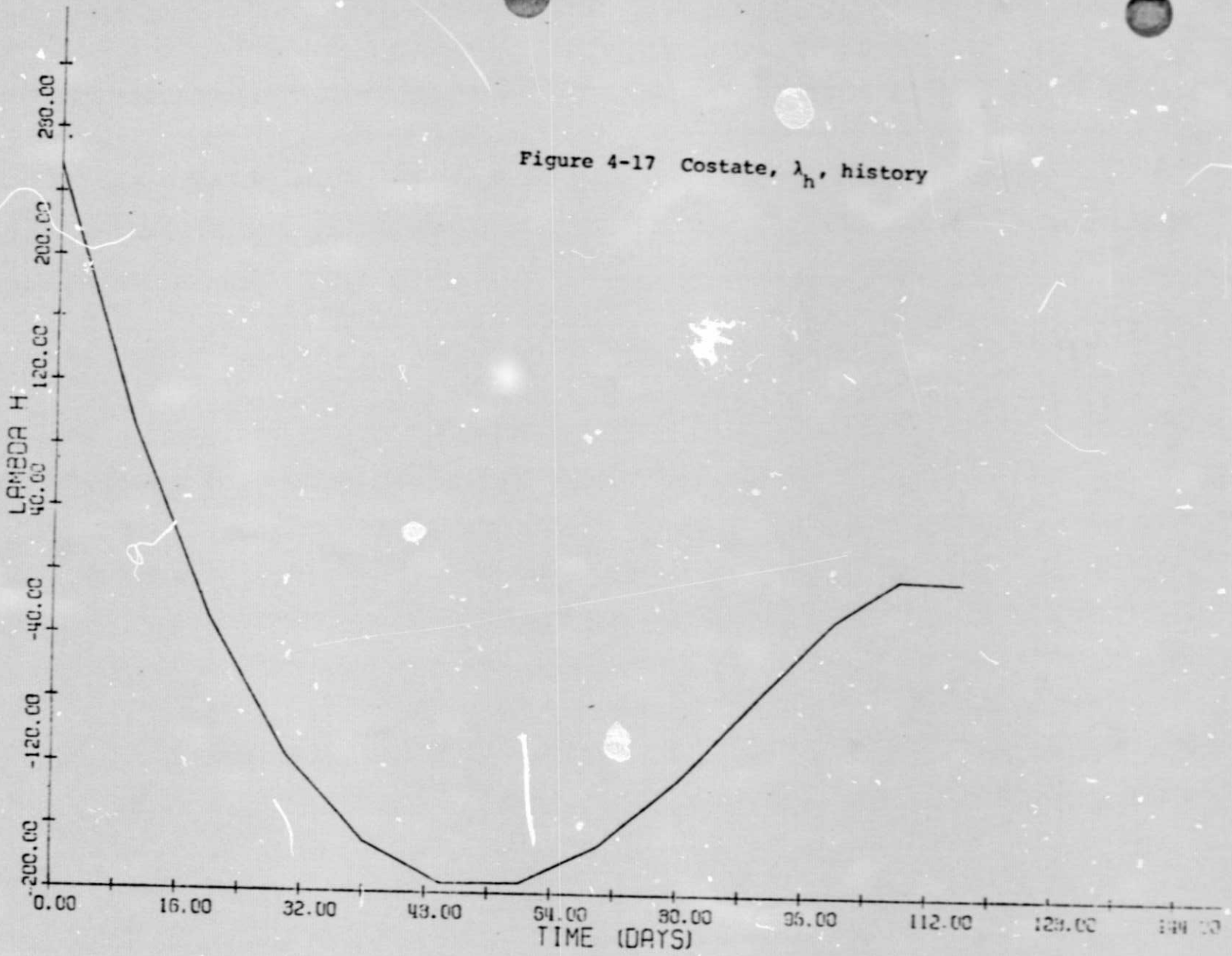

Figure 4-17 Costate, λ_h, history

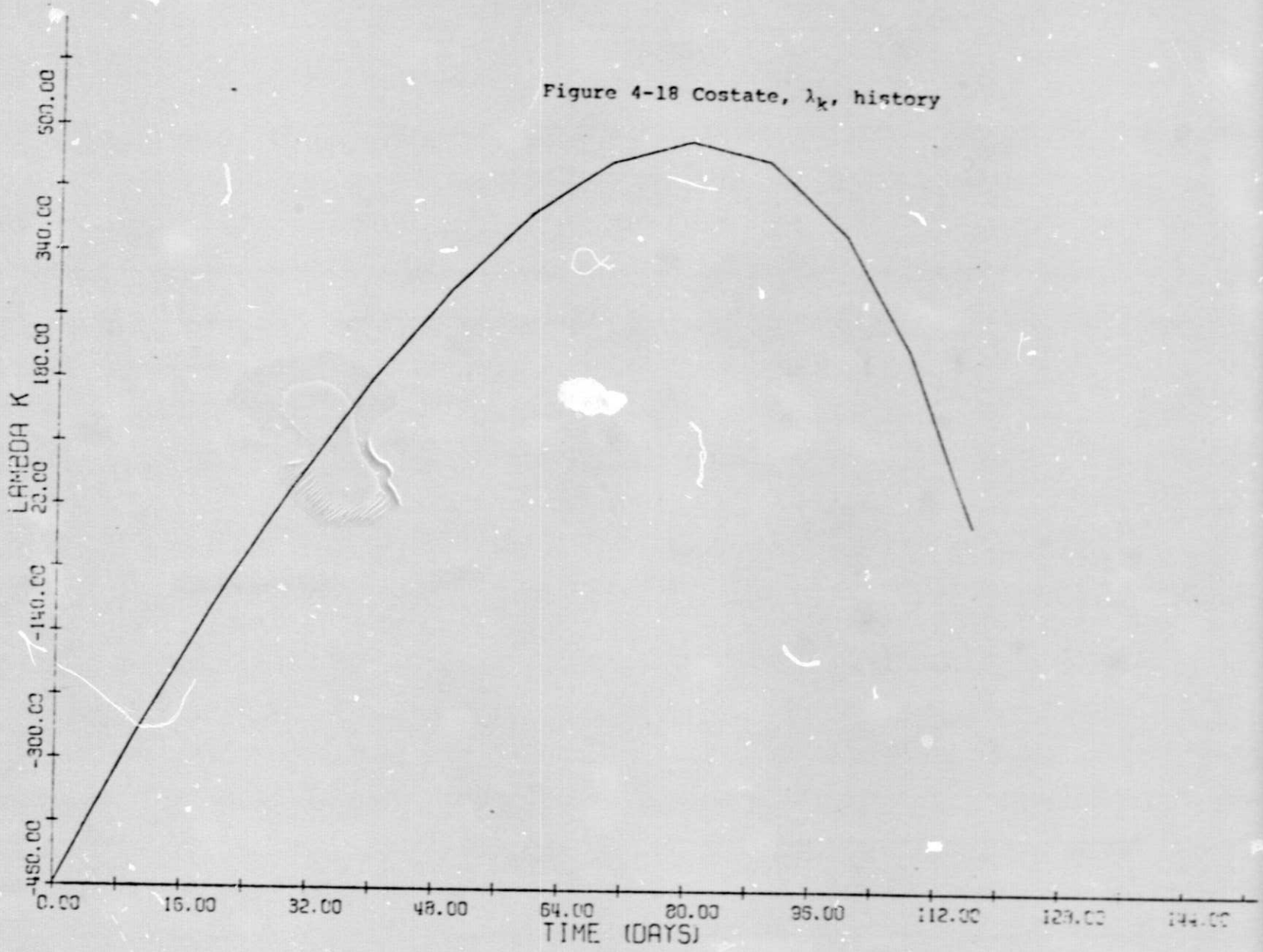

Figure 4-18 Costate, λ_k, history

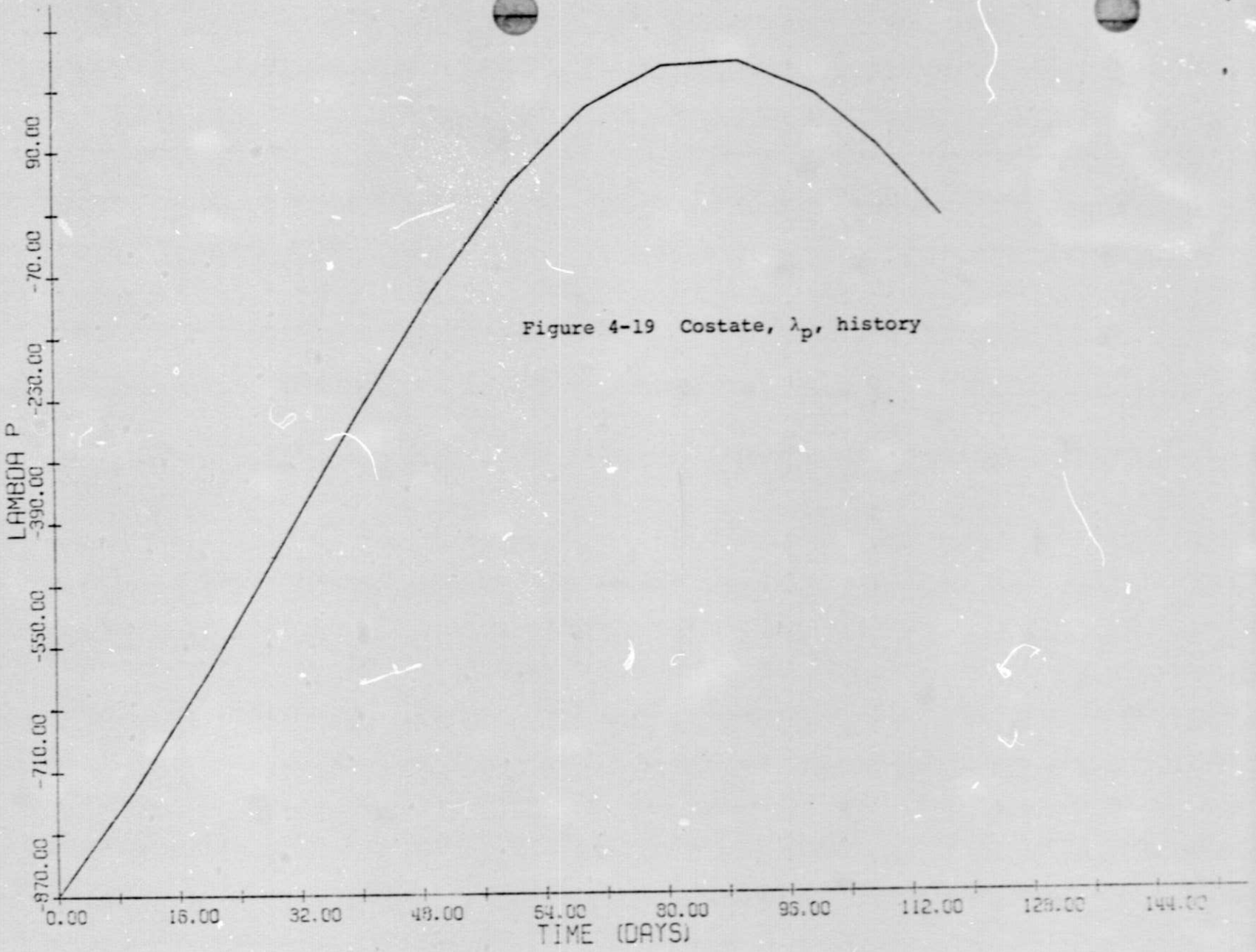

Figure 4-19 Costate, λ_p, history

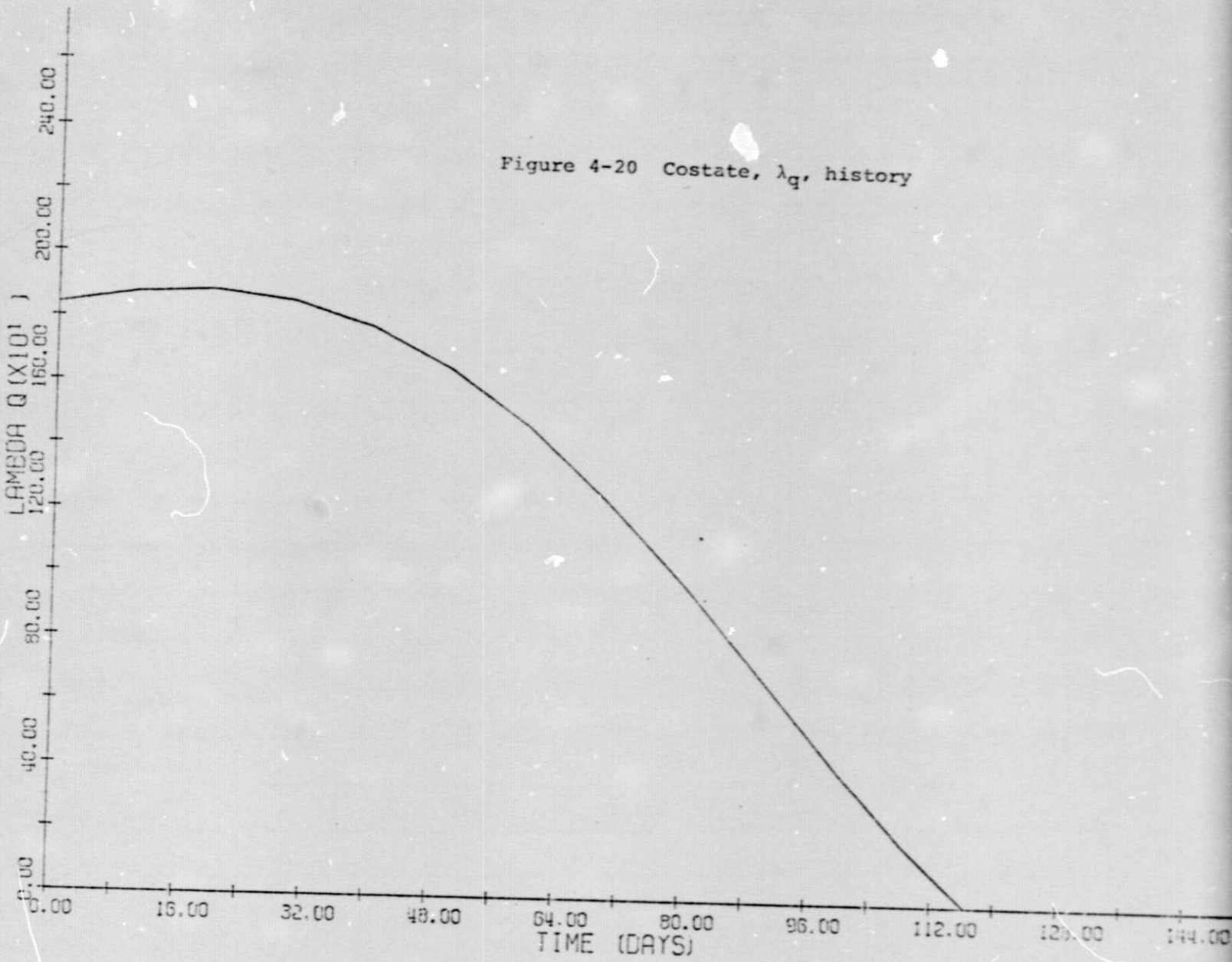

Figure 4-20 Costate, λ_q, history

Figure 4-21 Orbital period change

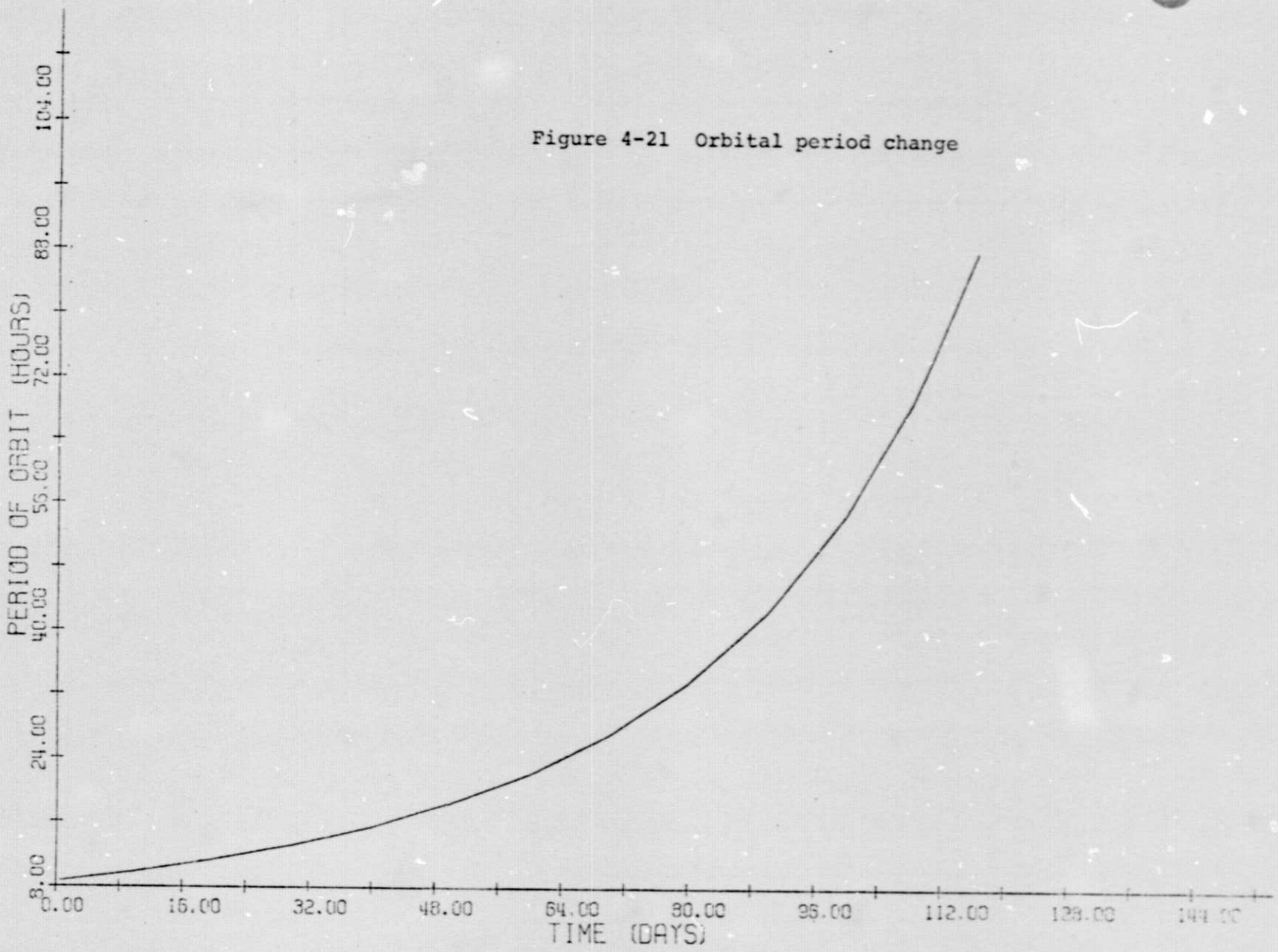

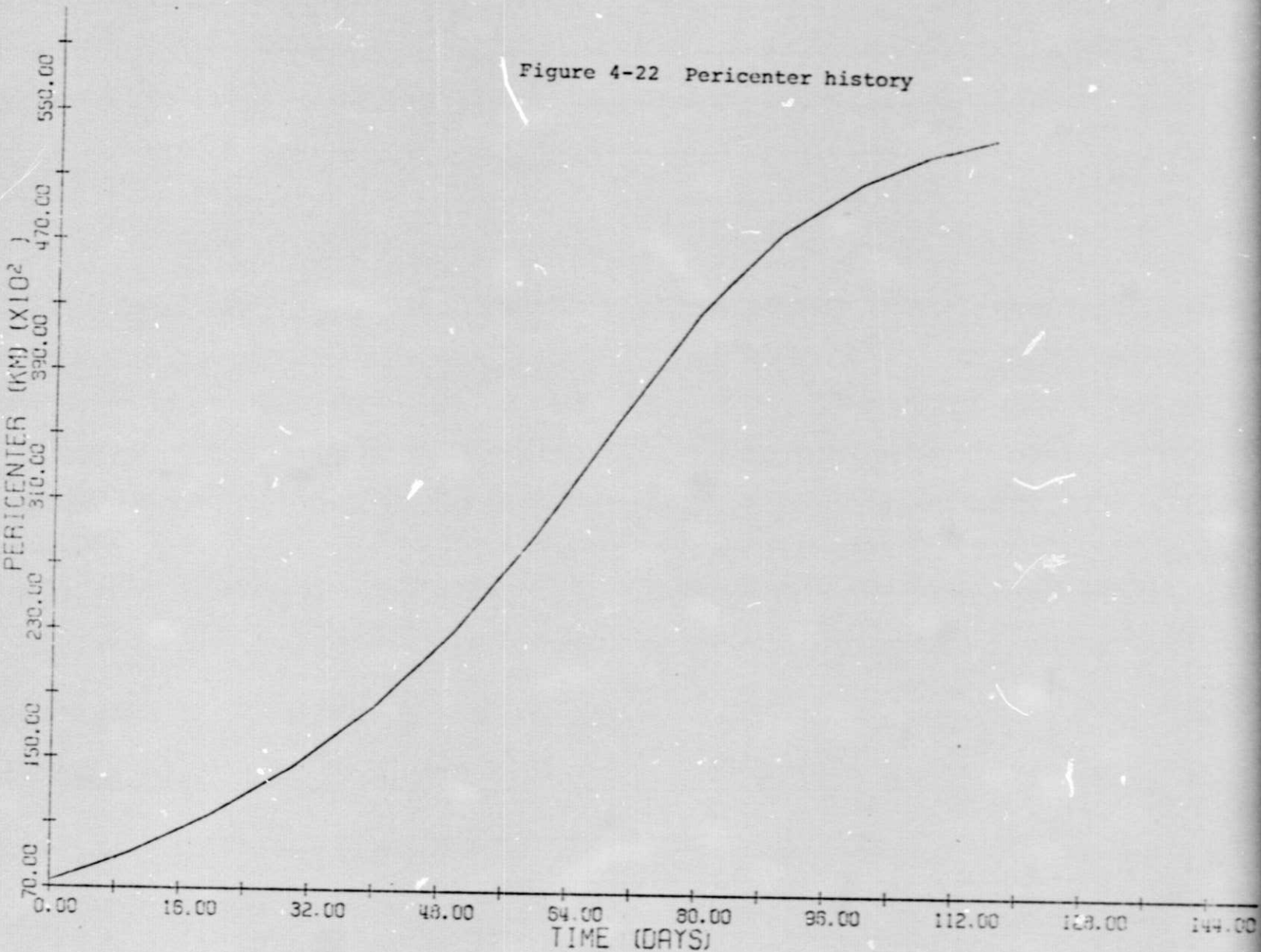

Figure 4-22 Pericenter history

Figure 4-23 Apocenter history

creased initially, reaching 4060 km at 110 days. In order to prevent the lowering of pericenter, a penalty function was added to the cost as discussed in Section 3. After some trial and error adjustment of the weighting factor between time and the penalty function, a trajectory was generated with a transfer time of 200.7 days with a minimum pericenter of 7650 km and a maximum eccentricity of 0.72. Thus the transfer time penalty was less than 3%. Figures 4-24 to 4-27 show the semimajor axis, eccentricity, inclination and pericenter histories for the case with the penalty function plus the pericenter history for the minimum time case. Although the trajectory was not changed very much, the costate histories were changed considerably. For example, the initial costate for the minimum time transfer was (5842, 3070, 3351, -5455, -4979). With the penalty function the initial costate was (9204, -372, 6533, -7903, -8536). It was necessary to perform a series of runs with increasing weighting factor in order to obtain convergence. The penalty function might be necessary for low altitude runs with shadowing since currently the shadow code is not valid for trajectories which intersect the planet's surface.

These results are meant to illustrate the capabilities of the program and, of course, do not represent an extensive performance study. Typical flight times are indicated, however, and show that the sail can reasonably be used for Earth escape and for orbit transfer.

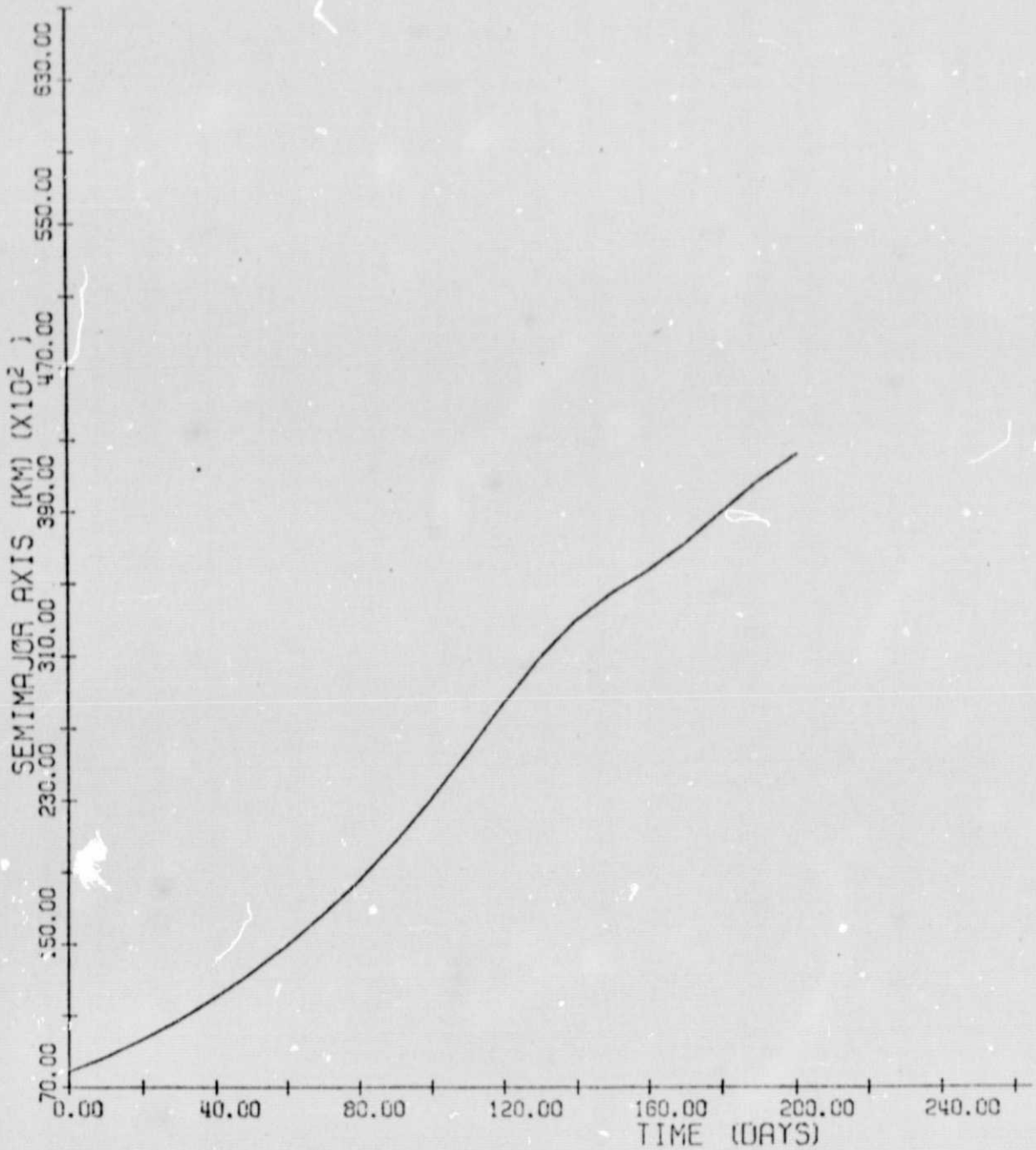

Figure 4-24 Semimajor axis history
Orbit transfer with penalty function

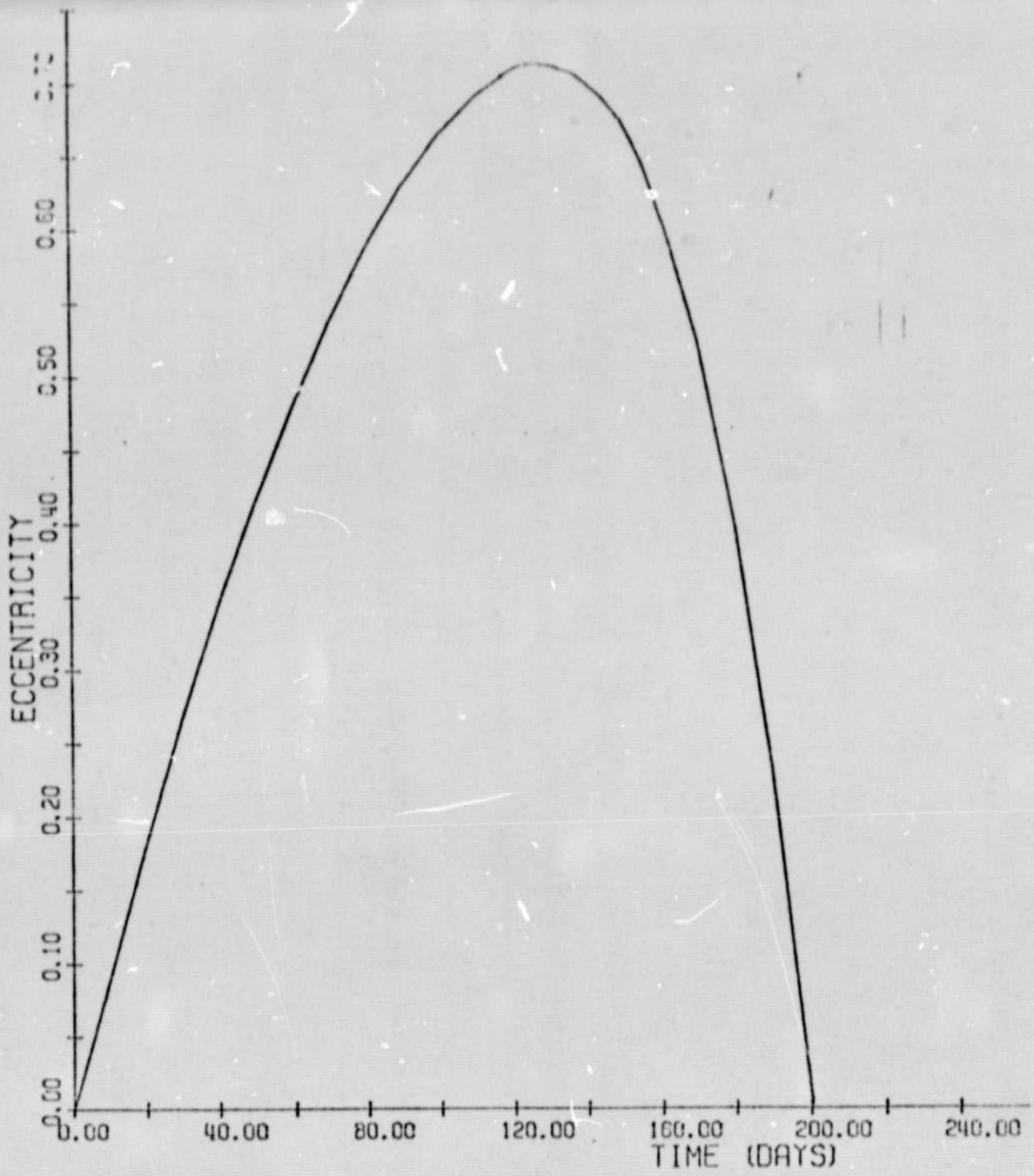

Figure 4-25 Eccentricity history
Orbit transfer with penalty function

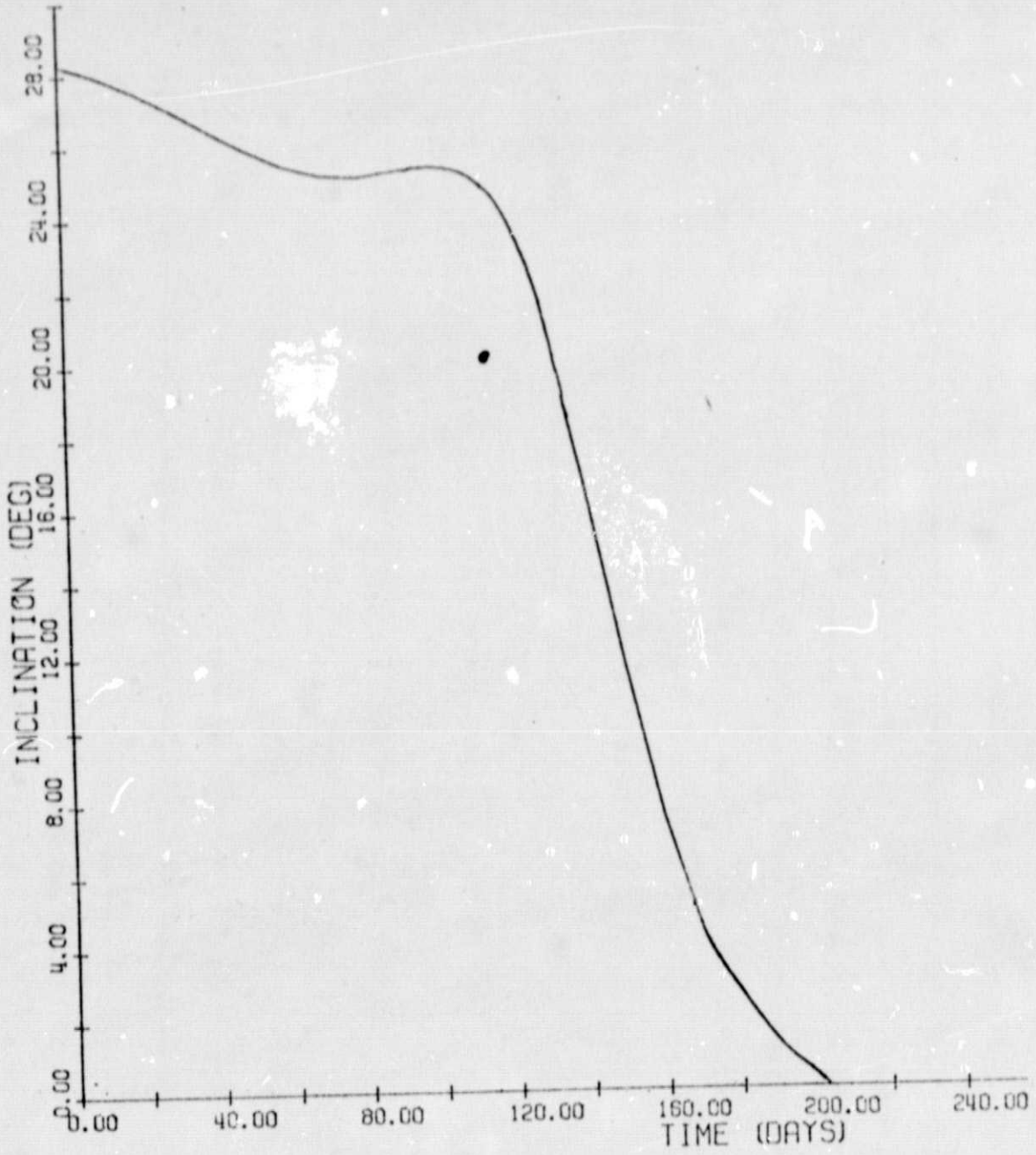

Figure 4-26 Inclination history
Orbit transfer with penalty function

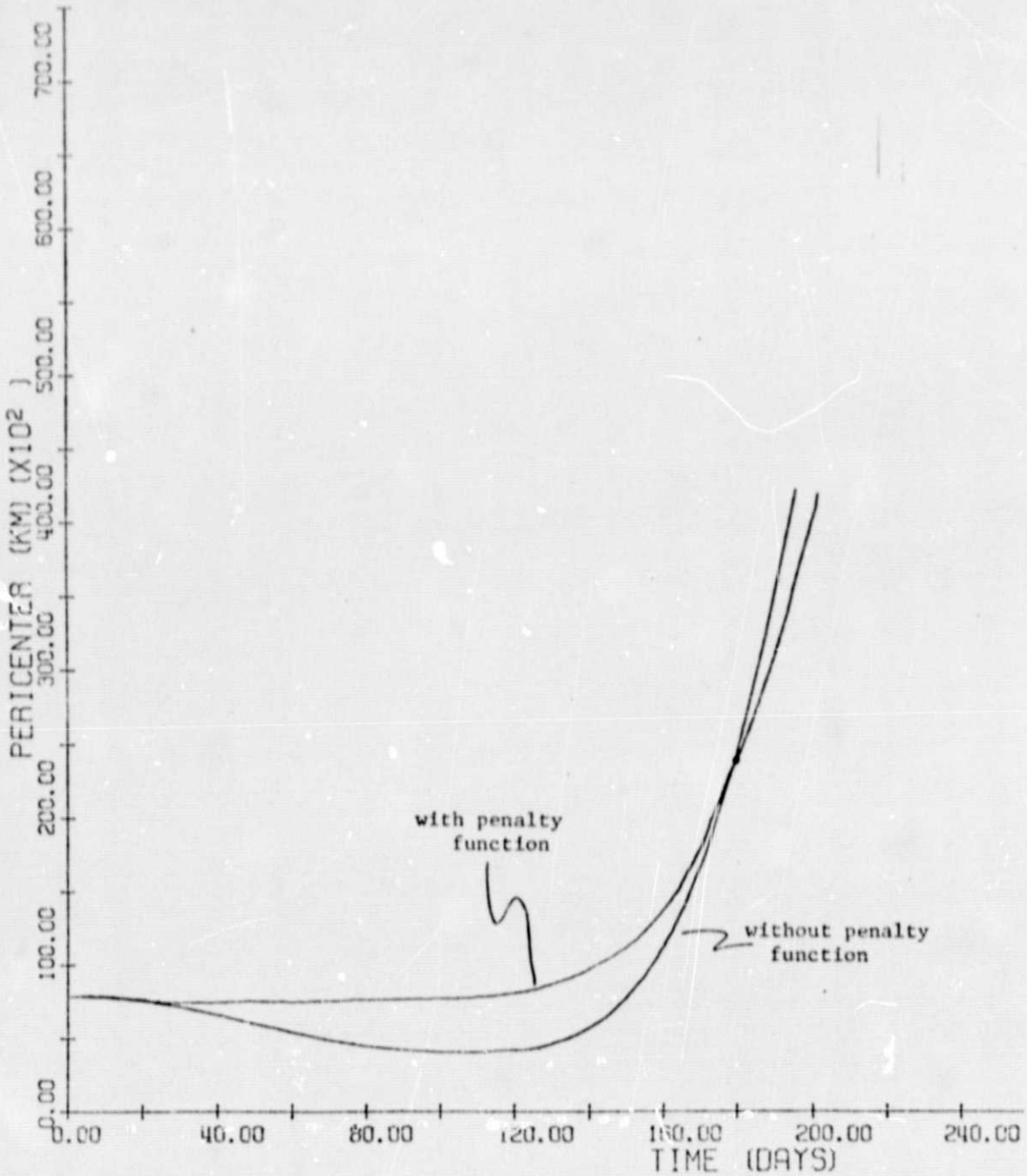

Figure 4-27 Pericenter history
With and without penalty function

SECTION 5

CONCLUDING REMARKS

A method for producing optimal solar sail planetocentric trajectories has been devised and implemented in a computer program called SUNSPOT. A square sail force model is assumed although it is similar to a simple heliogyro model. Ability to produce orbit to a subescape point and orbit to orbit transfer exists. The method of averaging allows rapid computation of trajectories, but since the thrust to weight ratio is assumed small, it does not allow trajectories to escape energy (infinite semimajor axis). The subescape point is defined as a large but finite semimajor axis. Typically one or two more revolutions would be required for escape and a suboptimal scheme can give easy and good estimates of the remaining flight time. In order to prevent intersection of a planet's surface, a penalty function may be included in the cost. Trajectories about the four inner planets can be generated.

The program is based on an earlier electric propulsion geocentric transfer program. As with the earlier work, shadowing, oblateness, and solar motion may be included. Equinoctial orbit elements are used to avoid singularities for zero eccentricity and inclination.

The optimization requires the solution of a two-point boundary-value problem. Several trajectories must be calculated to obtain convergence to the required boundary conditions. Each trajectory is calculated by integrating a first approximation to the state consisting of the orbital elements and the costate using a time step of several days. Averaging integrals are performed using a gaussian quadrature. Typically 16 points are used. In order to obtain convergence in a few iterations, a fairly good initial guess is required, especially for orbit-to-orbit transfer. Because the solar sail always has a component of force away from the sun, eccentricity tends to change quickly. Therefore, attainment of a particular final eccentricity can be difficult. Transfer to a subescape point did not present convergence difficulties.

A number of example trajectories were produced although a thorough performance analysis was not done because of changing conditions in the sail mission planning. Initial conditions on many of the cases were selected to take advantage of geometry to avoid the shadow and decrease flight time. Examples are for Earth orbital trajectories. Flight times are reasonable for a low thrust vehicle.

There are several possible extensions of this work. One is the inclusion of a more accurate heliogyro sail model. Planetshine effects may be important at low altitudes and for Mercury trajectories as indicated by some preliminary effort for this study. Attitude constraints, including rate and rate change constraints, are important. Such constraints were not included in the optimization although resulting trajectories can be inspected for violation of the constraints. Typically the constraints are violated during a segment of the orbit when the thrust is small compared to the rest of the orbit and so probably a suboptimal pointing would have a small effect. There is a tendency for eccentricity to become large so that intersections of the planet's surface occur. Currently, the shadow computations are not valid if this happens, causing an abort. A penalty function was used to prevent surface intersection for some examples, and there was only a small loss of performance. Obtaining convergence can be difficult, especially for orbit raising when a small final eccentricity is desired. For a complete escape trajectory a precision trajectory integration segment could be connected to the initial averaged section with the appropriate transition.

APPENDIX A

PRELIMINARY HELIOGYRO FORCE MODELING

Accurate force modeling of the heliogyro is very difficult. The force depends on the angular momentum vector, pitch angle, rotation angle, deformation etc. In an effort to produce a more simple model JPL obtained approximate thrust magnitude versus thrust vector cone angle values for various sun cone angles (i.e. the angle between the angular momentum vector or spin axis and the sun-line). Only data for zero collective pitch was obtained. Thus the sun-line, spin axis and thrust direction are assumed to lie in a plane. This data is reproduced in Table A-1 and this case is illustrated in Fig. A-1.

TABLE A-1

Values of Normalized Force Versus Force Cone Angle

(for two sun cone angles and for 0^{o} collective pitch; taken from JPL data)

Sun Cone Angle, α_p			Cyclic Pitch								
			0^{o}	10^{o}	20^{o}	30^{o}	40^{o}	-10^{o}	-20^{o}	-30^{o}	-40^{o}
0^{o}		F/F_p	.9012	.8849	.8376	.7648	.6744	.8849	.8376	.7648	.6744
		θ	0.0	-4.4753	-8.7425	-12.5642	-15.6465	+4.4753	+8.7425	+12.5642	+15.6465
15^{o}		F/F_p	.8469	.8649	.8578	.8186	.7535	.7877	.7114	.6203	.5244
		θ	+13.4921	+9.9253	+4.3073	-0.1556	-4.2282	+17.7996	+21.6079	+24.6206	+26.4823

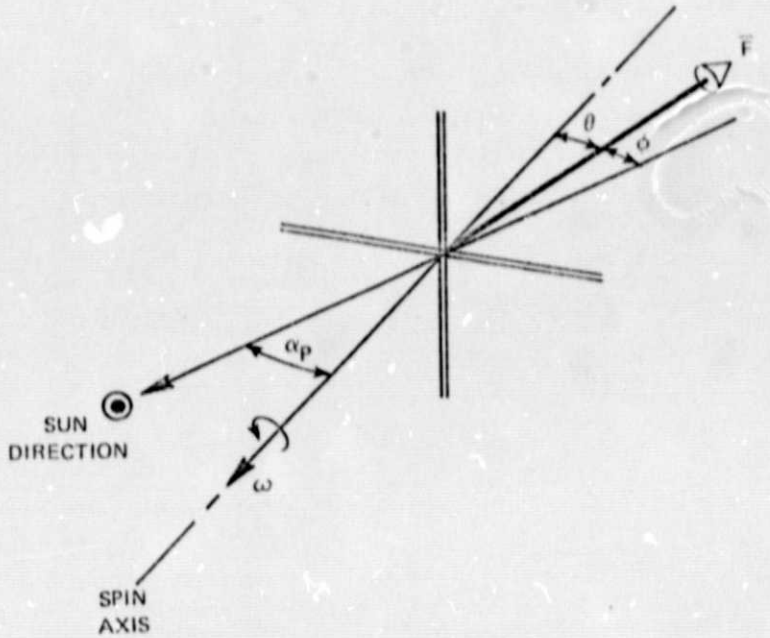

Figure A-1 Heliogyro Geometry

The spin vector direction can change only very slowly. As a first cut the data for zero sun cone angle was used to try to obtain values for coefficients using the square sail model. Since the data diverges considerably from a $\cos^2\theta$ curve, that form did not yield a good fit. A form using cos4θ and cos8θ did yield a very good fit. In particular let

$$\frac{F}{.9012} = 0.333+0.7709\cos4\theta-0.1042\ \cos8\theta \qquad (A.1)$$

Then Table A-2 shows a comparison of values from this formula with data from Table A-2. Note the cut-off angle of 30°:

TABLE A-2

Curve Fit Comparison

θ	$F_{data}/.9012$	$F_{calculated}/.9012$
0	1.0	1.0
4.4753	0.9819	0.9824
8.7425	0.9294	0.9293
12.5642	0.8486	0.8452
15.6465	0.7483	0.7483
20.	—	0.5651
25.	—	0.2974
30.	—	0.

Fig. A-2 illustrates the zero sun cone angle case for positive θ and using the curve fit of Eq. (A.1) to extrapolate the data to $\theta=30^{o}$. A curve is shown for the sun cone angle of 15^{o} also. No fit of the data to a mathematical expression was attempted for that case.

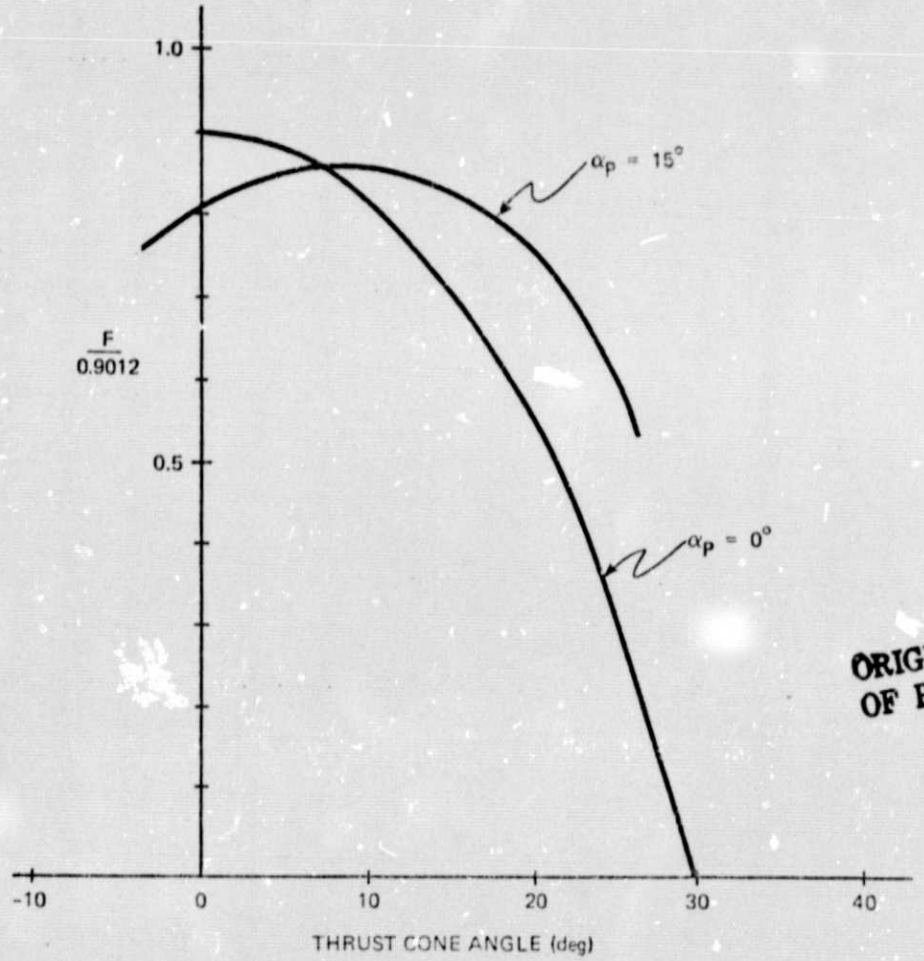

Figure A-2 Force magnitude variation with cone angle

APPENDIX B

THE MATRIX M AND ITS PARTIALS

Table B-1 Elements of M

$$M_{11} = \frac{2\dot{X}_1}{n^2 a}, \quad M_{12} = \frac{2\dot{Y}_1}{n^2 a}, \quad M_{13} = O$$

$$M_{21} = \frac{\sqrt{1-h^2-k^2}}{na^2}\left[\frac{\partial X_1}{\partial k} + \frac{\dot{X}_1}{n}(\sin F - h\beta)\right]$$

$$M_{22} = \frac{\sqrt{1-h^2-k^2}}{na^2}\left[\frac{\partial Y_1}{\partial k} + \frac{\dot{Y}_1}{n}(\sin F - h\beta)\right]$$

$$M_{23} = \frac{k(qY_1 - pX_1)}{na^2\sqrt{1-h^2-k^2}}$$

$$M_{31} = \frac{\sqrt{1-h^2-k^2}}{na^2}\left[\frac{\partial X_1}{\partial h} - \frac{\dot{X}_1}{n}(\cos F - k\beta)\right]$$

$$M_{32} = \frac{\sqrt{1-h^2-k^2}}{na^2}\left[\frac{\partial Y_1}{\partial h} - \frac{\dot{Y}_1}{n}(\cos F - k\beta)\right]$$

$$M_{33} = \frac{-h(qY_1 - pX_1)}{na^2\sqrt{1-h^2-k^2}}$$

$$M_{41} = O, \quad M_{42} = O, \quad M_{43} = \frac{(1+p^2+q^2)Y_1}{2na^2\sqrt{1-h^2-k^2}}$$

$$M_{51} = O, \quad M_{52} = O, \quad M_{53} = \frac{(1+p^2+q^2)X_1}{2na^2\sqrt{1-h^2-k^2}}$$

Table B-2 Partials of X_1 and Y_1 with Respect to h and k

$$\frac{\partial X_1}{\partial h} = a\left[-h\beta\cos F-(\beta+\frac{h^2\beta^3}{1-\beta})(h\cos F-k\sin F)\right]$$

$$\frac{\partial Y_1}{\partial h} = a\left[k\beta\cos F-1+\frac{hk\beta^3}{1-\beta}(h\cos F-k\sin F)\right]$$

$$\frac{\partial X_1}{\partial k} = a\left[h\beta\sin F-1-\frac{hk\beta^3}{1-\beta}(h\cos F-k\sin F)\right]$$

$$\frac{\partial Y_1}{\partial k} = a\left[-k\beta\sin F+(\beta+\frac{k^2\beta^3}{1-\beta})(h\cos F-k\sin F)\right]$$

Table B-3 Partial of M with Respect to a

$$\frac{\partial M}{\partial a} = \frac{1}{2a}\begin{bmatrix}3&0&0&0&0\\0&1&0&0&0\\0&0&1&0&0\\0&0&0&1&0\\0&0&0&0&1\end{bmatrix} M$$

Table B-4 Partial of M with Respect to h

$$\frac{\partial M_{11}}{\partial h} = \frac{2}{n^2 a}\frac{\partial \dot{X}_1}{\partial h}, \quad \frac{\partial M_{12}}{\partial h} = \frac{2}{n^2 a}\frac{\partial \dot{Y}_1}{\partial h}, \quad \frac{\partial M_{13}}{\partial h} = 0$$

$$\frac{\partial M_{21}}{\partial h} = \frac{-hM_{21}}{1-h^2-k^2} + \frac{\sqrt{1-h^2-k^2}}{na^2}\left[\frac{\partial^2 X_1}{\partial h \partial k} + \frac{\partial \dot{X}_1}{\partial h}\frac{(\sin F - h\beta)}{n} - \frac{\dot{X}_1}{n}\frac{(\beta+h^2\beta^3)}{1-\beta}\right]$$

$$\frac{\partial M_{22}}{\partial h} = \frac{-hM_{22}}{1-h^2-k^2} + \frac{\sqrt{1-h^2-k^2}}{na^2}\left[\frac{\partial^2 Y_1}{\partial h \partial k} + \frac{\partial \dot{Y}_1}{\partial h}\frac{(\sin F - h\beta)}{n} - \frac{\dot{Y}_1}{n}\frac{(\beta+h^2\beta^3)}{1-\beta}\right]$$

$$\frac{\partial M_{23}}{\partial h} = \frac{hM_{23}}{1-h^2-k^2} + \frac{k}{na^2\sqrt{1-h^2-k^2}}\left(q\frac{\partial Y_1}{\partial h} - p\frac{\partial X_1}{\partial h}\right)$$

$$\frac{\partial M_{31}}{\partial h} = \frac{-hM_{31}}{1-h^2-k^2} - \frac{\sqrt{1-h^2-k^2}}{na^2}\left[\frac{\partial^2 X_1}{\partial h^2} - \frac{\partial \dot{X}_1}{\partial h}\frac{(\cos F - k\beta)}{n} + \frac{\dot{X}_1}{n}\frac{hk\beta^3}{1-\beta}\right]$$

$$\frac{\partial M_{32}}{\partial h} = \frac{-hM_{32}}{1-h^2-k^2} - \frac{\sqrt{1-h^2-k^2}}{na^2}\left[\frac{\partial^2 Y_1}{\partial h^2} - \frac{\partial \dot{Y}_1}{\partial h}\frac{(\cos F - k\beta)}{n} + \frac{\dot{Y}_1}{n}\frac{hk\beta^3}{1-\beta}\right]$$

$$\frac{\partial M_{33}}{\partial h} = \frac{hM_{33}}{1-h^2-k^2} + \frac{M_{33}}{h} - \frac{h}{na^2\sqrt{1-h^2-k^2}}\left(q\frac{\partial Y_1}{\partial h} - p\frac{\partial X_1}{\partial h}\right)$$

$$\frac{\partial M_{41}}{\partial h} = 0, \quad \frac{\partial M_{42}}{\partial h} = 0, \quad \frac{\partial M_{43}}{\partial h} = \frac{hM_{43}}{1-h^2-k^2} + \frac{M_{43}}{Y_1}\frac{\partial Y_1}{\partial h}$$

$$\frac{\partial M_{51}}{\partial h} = 0, \quad \frac{\partial M_{52}}{\partial h} = 0, \quad \frac{\partial M_{53}}{\partial h} = \frac{hM_{53}}{1-h^2-k^2} + \frac{M_{53}}{X_1}\frac{\partial X_1}{\partial h}$$

Table B-5 Partial of M with Respect to k

$$\frac{\partial M_{11}}{\partial k} = \frac{2}{n^2 a}\frac{\partial \dot{X}_1}{\partial k}, \quad \frac{\partial M_{12}}{\partial k} = \frac{2}{n^2 a}\frac{\partial \dot{Y}_1}{\partial k}, \quad \frac{\partial M_{13}}{\partial k} = 0$$

$$\frac{\partial M_{21}}{\partial k} = \frac{-kM_{21}}{1-h^2-k^2} + \frac{\sqrt{1-h^2-k^2}}{na^2}\left[\frac{\partial^2 X_1}{\partial k^2} + \frac{\partial \dot{X}_1}{\partial k}\frac{(\sin F - h\beta)}{n} - \frac{\dot{X}_1}{n}\frac{hk\beta^3}{1-\beta}\right]$$

$$\frac{\partial M_{22}}{\partial k} = \frac{-kM_{22}}{1-h^2-k^2} + \frac{\sqrt{1-h^2-k^2}}{na^2}\left[\frac{\partial^2 Y_1}{\partial k^2} + \frac{\partial \dot{Y}_1}{\partial k}\frac{(\sin F - h\beta)}{n} - \frac{\dot{Y}_1}{n}\frac{hk\beta^3}{1-\beta}\right]$$

$$\frac{\partial M_{23}}{\partial k} = \frac{M_{23}}{k} + \frac{kM_{23}}{1-h^2-k^2} + \frac{k}{na^2\sqrt{1-h^2-k^2}}\left(q\frac{\partial Y_1}{\partial k} - p\frac{\partial X_1}{\partial k}\right)$$

$$\frac{\partial M_{31}}{\partial k} = -\frac{kM_{31}}{1-h^2-k^2} - \frac{\sqrt{1-h^2-k^2}}{na^2}\left[\frac{\partial^2 X_1}{\partial k \partial h} - \frac{\partial \dot{X}_1}{\partial k}\left(\frac{\cos F - k\beta}{n}\right) + \frac{\dot{X}_1}{n}\frac{(\beta + k^2\beta^3)}{1-\beta}\right]$$

$$\frac{\partial M_{32}}{\partial k} = \frac{-kM_{32}}{1-h^2-k^2} - \frac{\sqrt{1-h^2-k^2}}{na^2}\left[\frac{\partial^2 Y_1}{\partial k \partial h} - \frac{\partial \dot{Y}_1}{\partial k}\left(\frac{\cos F - k\beta}{n}\right) + \frac{\dot{Y}_1}{n}\frac{(\beta + k^2\beta^3)}{1-\beta}\right]$$

$$\frac{\partial M_{33}}{\partial k} = \frac{kM_{33}}{1-h^2-k^2} - \frac{h}{na^2\sqrt{1-h^2-k^2}}\left(q\frac{\partial Y_1}{\partial k} - p\frac{\partial X_1}{\partial k}\right)$$

$$\frac{\partial M_{41}}{\partial k} = 0, \quad \frac{\partial M_{42}}{\partial k} = 0, \quad \frac{\partial M_{43}}{\partial k} = \frac{kM_{43}}{1-h^2-k^2} + \frac{M_{43}}{Y_1}\frac{\partial Y_1}{\partial k}$$

$$\frac{\partial M_{51}}{\partial k} = 0, \quad \frac{\partial M_{52}}{\partial k} = 0, \quad \frac{\partial M_{53}}{\partial k} = \frac{kM_{53}}{1-h^2-k^2} + \frac{M_{53}}{X_1}\frac{\partial X_1}{\partial k}$$

Table B-6 Non-zero Partials of M with Respect to p

$$\frac{\partial M_{23}}{\partial p} = \frac{-kX_1}{\sqrt{1-h^2-k^2}\ na^2}$$

$$\frac{\partial M_{33}}{\partial p} = \frac{hX_1}{\sqrt{1-h^2-k^2}\ na^2}$$

$$\frac{\partial M_{43}}{\partial p} = \frac{pY_1}{\sqrt{1-h^2-k^2}\ na^2}$$

$$\frac{\partial M_{53}}{\partial p} = \frac{pX_1}{\sqrt{1-h^2-k^2}\ na^2}$$

Table B-7 Non-zero Partials of M with Respect to q

$$\frac{\partial M_{23}}{\partial q} = \frac{kY_1}{\sqrt{1-h^2-k^2}\ na^2}$$

$$\frac{\partial M_{33}}{\partial q} = \frac{-hY_1}{\sqrt{1-h^2-k^2}\ na^2}$$

$$\frac{\partial M_{43}}{\partial q} = \frac{qY_1}{\sqrt{1-h^2-k^2}\ na^2}$$

$$\frac{\partial M_{53}}{\partial q} = \frac{qX_1}{\sqrt{1-h^2-k^2}\ na^2}$$

Table B-8 Partials of $\dot{X}_1$ and $\dot{Y}_1$ with Respect to h and k

$$\frac{\partial \dot{X}_1}{\partial h} = \frac{a}{r}\dot{X}_1 \sin F + \frac{na^2}{r}\left[(h\sin F + k\cos F)\left(\beta + \frac{h^2\beta^3}{1-\beta}\right) + h\beta\sin F\right]$$

$$\frac{\partial \dot{Y}_1}{\partial h} = \frac{a}{r}\dot{Y}_1 \sin F + \frac{na^2}{r}\left[-k\beta\sin F - \frac{hk\beta^3}{1-\beta}(h\sin F + k\cos F)\right]$$

$$\frac{\partial \dot{X}_1}{\partial k} = \frac{a}{r}\dot{X}_1 \cos F + \frac{na^2}{r}\left[h\beta\cos F + \frac{hk\beta^3}{1-\beta}(h\sin F + k\cos F)\right]$$

$$\frac{\partial \dot{Y}_1}{\partial k} = \frac{a}{r}\dot{Y}_1 \cos F + \frac{na^2}{r}\left[-(h\sin F + k\cos F)\left(\beta + \frac{k^2\beta^3}{1-\beta}\right) + k\beta\cos F\right]$$

Table B-9 Second Partials of X_1 and Y_1 with Respect to h and k

$$\frac{\partial^2 X_1}{\partial h^2} = a\left[\frac{h\beta^3}{1-\beta}(-h\cos F + k\sin F)\left(3 + h^2\beta^2\frac{(3-2\beta)}{(1-\beta)^2}\right) - 2\cos F\left(\beta + \frac{h^2\beta^3}{1-\beta}\right)\right]$$

$$\frac{\partial^2 Y_1}{\partial h^2} = a\left[\frac{k\beta^3}{1-\beta}(h\cos F - k\sin F)\left(1 + h^2\frac{(3\beta^2-2\beta^3)}{(1-\beta)^2}\right) + \frac{2hk\beta^3}{1-\beta}\cos F\right]$$

$$\frac{\partial^2 X_1}{\partial k^2} = a\left[\frac{h\beta^3}{1-\beta}(-h\cos F + k\sin F)\left(1 + k^2\frac{(3\beta^2-2\beta^3)}{(1-\beta)^2}\right) + \frac{2hk\beta^3}{1-\beta}\sin F\right]$$

$$\frac{\partial^2 Y_1}{\partial k^2} = a\left[\frac{k\beta^3}{1-\beta}(h\cos F - k\sin F)\left(3 + k^2\frac{(3\beta^2-2\beta^3)}{(1-\beta)^2}\right) - 2\sin F\left(\beta + \frac{k^2\beta^3}{1-\beta}\right)\right]$$

$$\frac{\partial^2 X_1}{\partial h \partial k} = \frac{\partial^2 X_1}{\partial k \partial h} = a\left[\frac{k\beta^3}{1-\beta}(-h\cos F + k\sin F)\left(1 + h^2\frac{(3\beta^2-2\beta^3)}{(1-\beta)^2}\right) - \frac{hk\beta^3}{1-\beta}\cos F + \sin F\left(\beta + \frac{h^2\beta^3}{1-\beta}\right)\right]$$

$$\frac{\partial^2 Y_1}{\partial k \partial h} = \frac{\partial^2 Y_1}{\partial h \partial k} = a\left[\frac{h\beta^3}{1-\beta}(h\cos F - k\sin F)\left(1 + k^2\frac{(3\beta^2-2\beta^3)}{(1-\beta)^2}\right) - \frac{hk\beta^3}{1-\beta}\sin F + \cos F\left(\beta + \frac{k^2\beta^3}{1-\beta}\right)\right]$$

APPENDIX C

SINGLE AVERAGED OBLATENESS EQUATIONS

In these equations R_e is the earth's radius, μ is the gravitational constant, n is the orbital angular speed, J_2 the oblateness coefficient and a, h, k, p, q the equinoctial orbital elements.

Table C-1 J_2 Variation of Parameters Equations

$$\dot{h}_{J_2} = \frac{3\mu R_e^2 J_2 k\left[1-6(1^2+q^2)+3(p^2+q^2)^2\right]}{2na^5(1-h^2-k^2)\,(1+p^2+q^2)^2}$$

$$\dot{k}_{J_2} = \frac{3\mu R_e^2 J_2 h\left[1-6(p^2+q^2)+3(p^2+q^2)^2\right]}{2na^5(1-h^2-k^2)^2\,(1+p^2+q^2)^2}$$

$$\dot{p}_{J_2} = \frac{3\mu R_e^2 J_2 q(1-p^2-q^2)}{2na^5(1-h^2-k^2)^2\,(1+p^2+q^2)}$$

$$\dot{q}_{J_2} = \frac{3\mu R_e^2 J_2 p(1-p^2-q^2)}{2na^5(1-h^2-k^2)^2\,(1+p^2+q^2)}$$

Table C-2 Partial of J_2 Equations with Respect to a

$$\frac{\partial \dot{h}}{\partial a} = -\frac{7}{2}\frac{\dot{h}}{a}$$

$$\frac{\partial \dot{k}}{\partial a} = -\frac{7}{2}\frac{\dot{k}}{a}$$

$$\frac{\partial \dot{p}}{\partial a} = -\frac{7}{2}\frac{\dot{p}}{a}$$

$$\frac{\partial \dot{q}}{\partial a} = -\frac{7}{2}\frac{\dot{q}}{a}$$

Table C-3 Partial of J_2 Equations with Respect to h

$$\frac{\partial \dot{h}}{\partial h} = \frac{4h\dot{h}}{1-h^2-k^2}$$

$$\frac{\partial \dot{k}}{\partial h} = \frac{\dot{k}}{h} + \frac{4h\dot{k}}{1-h^2-k^2}$$

$$\frac{\partial \dot{p}}{\partial h} = \frac{4h\dot{p}}{1-h^2-k^2}$$

$$\frac{\partial \dot{q}}{\partial h} = \frac{4h\dot{q}}{1-h^2-k^2}$$

Table C-4 Partial of J_2 Equations with Respect to k

$$\frac{\partial \dot{h}}{\partial k} = \frac{\dot{h}}{k} + \frac{4k\dot{h}}{1-h^2-k^2}$$

$$\frac{\partial \dot{k}}{\partial k} = \frac{4k\dot{k}}{1-h^2-k^2}$$

$$\frac{\partial \dot{p}}{\partial k} = \frac{4k\dot{p}}{1-h^2-k^2}$$

$$\frac{\partial \dot{q}}{\partial k} = \frac{4k\dot{q}}{1-h^2-k^2}$$

Table C-5 Partial of J_2 Equations with Respect to p

$$\frac{\partial \dot{h}}{\partial p} = \left(\frac{12\mu R_e^2 J_2}{na^5}\right) \frac{kp(3(p^2+q^2)-2)}{(1-h^2-k^2)^2\,(1+p^2+q^2)^3}$$

$$\frac{\partial \dot{k}}{\partial p} = \left(\frac{12\mu R_e^2 J_2}{na^5}\right) \frac{hp(3(p^2+q^2)-2)}{(1-h^2-k^2)^2\,(1+p^2+q^2)^3}$$

$$\frac{\partial \dot{p}}{\partial p} = \frac{-2\dot{p}}{1-(p^2+q^2)^2}$$

$$\frac{\partial \dot{q}}{\partial p} = \frac{-\dot{q}}{p}\left[\frac{1+(p^2+q^2)^2}{1-(p^2+q^2)^2}\right]$$

Table C-6 Partial of J_2 Equations with Respect to q

$$\frac{\partial \dot{h}}{\partial q} = \left(\frac{12\mu R_e^2 J_2}{na^5}\right) \frac{kq(3(p^2+q^2)-2)}{(1-h^2-k^2)^2\,(1+p^2+q^2)^3}$$

$$\frac{\partial \dot{k}}{\partial q} = \left(\frac{12\mu R_e^2 J_2}{na^5}\right) \frac{hq(3(p^2+q^2)-2)}{(1-h^2-k^2)^2\,(1+p^2+q^2)^3}$$

$$\frac{\partial \dot{p}}{\partial q} = \frac{-\dot{p}}{q}\left[\frac{1+(p^2+q^2)^2}{1-(p^2+q^2)^2}\right]$$

$$\frac{\partial \dot{q}}{\partial q} = \frac{-2\dot{q}}{1-(p^2+q^2)^2}$$

APPENDIX D

SHADOW CALCULATIONS

This appendix essentially reproduces the summary of shadowing results from Ref. 12. From geometrical considerations an equation can be derived which the entry and exit angles must satisfy. Such an equation is given in Reference 28 and the equation given in this section is essentially the same, except that it is given in terms of equinoctial orbital elements.

The spacecraft position is given by

$$\underline{r} = X_1\hat{\underline{f}} + Y_1\hat{\underline{g}} \tag{D.1}$$

where X_1 and Y_1 were given in Eq. (3.16) and (3.17). Let the unit vector from the planet to the sun be given by

$$\hat{\underline{R}}_s = X_s\hat{\underline{f}} + Y_s\hat{\underline{g}} + Z_s\hat{\underline{w}}$$

This is in terms of the equinoctial coordinate frome and thus depends on the equinoctial orbital elements p and q. The calculation of the sun's direction in the equinoctial coordinate system is discussed in Section 3. If a_e designates the planet's radius, the cosine of the angle between $\underline{r}$ and $\hat{\underline{R}}_s$ is given by

$$\frac{\hat{\underline{R}}_s \cdot \underline{r}}{|\underline{r}|} = -\frac{(|\underline{r}|^2 - a_e^2)^{1/2}}{|\underline{r}|} \tag{D.2}$$

or,

$$X_1X_s + Y_1Y_s = -(|\underline{r}|^2 - a_e^2)^{1/2} \tag{D.3}$$

Squaring and rearranging

$$S \equiv (1-X_s^2)X_1^2 + (1-Y_s^2)Y_1^2 = 2X_sY_sX_1Y_1 - a_e^2 = 0 \tag{D.4}$$

This is the shadow equation which must be satisfied by the entry and exit angles. X_1 and Y_1 are functions of cosF, sinF, a, h, and k (see Eq. (3.16) and (3.17). By further manipulations one can derive a quartic equation in cosF. The coefficients of this quartic equation are given in Table D-1. Spurious roots can be eliminated by the criteria that $S = 0$ and that $\underline{R} \cdot \underline{r} < 0$. In addition, for the entry angle $\partial S/\partial F < 0$ and for the exit angle $\partial S/\partial F > 0$.

Table D-1 The Shadow Quartic Equation

$$b_1 = 1-h^2\beta$$

$$b_2 = hk\beta$$

$$b_3 = 1-k^2\beta$$

$$d_1 = 1-X_s^2$$

$$d_2 = 1-Y_s^2$$

$$d_3 = 2Y_sX_s$$

$$h_1 = d_1(b_1^2-b_2^2) + d_2(b_2^2-b_3^2) - d_3(b_1b_2-b_2b_3)$$

$$h_2 = -2d_1kb_1-2d_2hb_2+d_3(kb_2+hb_1)$$

$$h_3 = d_1(b_2+k^2)+d_2(b_3^2+h^2)-d_3(b_2b_3+hk) - \frac{a_e^2}{a^2}$$

$$h_4 = 2b_1b_2d_1+2b_2b_3-d_3(b_2^2+b_1b_3)$$

$$h_5 = -2kb_2d_1 - 2hb_3d_2 + d_3(kb_3+hb_2)$$

$$A_0 = h_1^2 + h_4^2$$

$$A_1 = 2h_1h_2 + 2h_4h_5$$

$$A_2 = h_2^2 + 2h_3h_1 - h_4^2 + h_5^2$$

$$A_3 = 2h_3h_2 - 2h_4h_5$$

$$A_4 = h_3^2 - h_5^2$$

$$S = A_0\cos^4F+A_1\cos^3F+A_2\cos^2F+A_3\cosF+A_4 = 0$$

Derivatives of F and S

The derivative of F with respect to $\underline{z}$ is needed to evaluate the costate equation. It can be obtained implicitly from the shadow equation.

$$\frac{dF}{d\underline{z}} = -\frac{\partial S}{\partial \underline{z}} \Big/ \frac{\partial S}{\partial F} \qquad (D.5)$$

These partials are listed in Table D-2. Note that in calculating $\partial S/\partial p$ and $\partial S/\partial q$ we have taken into account the fact that the sun's direction is given in equinoctial coordinates.

Table D-2 Partials of the Shadow Function

$$\frac{\partial S}{\partial F} = 2\left[(1-X_s^2)X_1 - X_s Y_s Y_1\right]\frac{\partial X_1}{\partial F} + 2\left[(1-Y_s^2)Y_1 - X_s Y_s Y_1\right]\frac{\partial Y_1}{\partial F}$$

$$\frac{\partial X_1}{\partial F} = a\left[-(1-h^2\beta)\sin F + hk\beta\cos F\right]$$

$$\frac{\partial Y_1}{\partial F} = a\left[-hk\beta\sin F + (1-k^2\beta)\cos F\right]$$

$$\frac{\partial S}{\partial a} = \frac{2a_e^2}{a}$$

$$\frac{\partial S}{\partial h} = 2\left[(1-X_s^2)X_1 - X_s Y_s Y_1\right]\frac{\partial X_1}{\partial h} + 2\left[(1-Y_s^2)Y_1 - X_s Y_s X_1\right]\frac{\partial Y_1}{\partial k}$$

$$\frac{\partial S}{\partial k} = 2\left[(1-X_s^2)X_1 - X_s Y_s Y_1\right]\frac{\partial X_1}{\partial k} + 2\left[(1-Y_s^2)Y_1 - X_s Y_s Y_1\right]\frac{\partial Y_1}{\partial k}$$

$$\frac{\partial S}{\partial p} = -4\left[X_1^2 X_s + X_1 Y_1 Y_s\right]\left[\frac{qY_s + Z_s}{1+p^2+q^2}\right] - 4\left[Y_1^2 Y_s + X_1 Y_1 X_s\right]\left[\frac{qX_s}{1+p^2+q^2}\right]$$

$$\frac{\partial S}{\partial q} = -4\left[X_1^2 X_s + X_1 Y_1 Y_s\right]\left[\frac{pY_s}{1+p^2+q^2}\right] - 4\left[Y_1^2 Y_s + X_1 Y_1 X_s\right]\left[\frac{-pX_s + Z_s}{1+p^2+q^2}\right]$$

APPENDIX E

A STRATEGY WHICH MAXIMIZES MEAN RATE-OF-CHANGE OF ENERGY

As part of a solar sail planetocentric performance analysis, a strategy was developed, coded, and run to produce trajectories which maximize the mean orbital rate-of-change of energy locally. The computer program (SUNSPOT), which was being developed to produce minimum time escape trajectories, was modified to produce a number of trajectories using this strategy.

The computer code, which uses the method of averaging, is valid for the spiral phase only. The averaging method is valid only if the thrust/weight ratio is small. Therefore the trajectories cannot be extended to escape energy ($C_3 = 0$).

Although the computer program is designed to solve a two point boundary-value problem, single trajectories can be produced. The state and costate equations are integrated, starting at a specified initial orbit, for a specified length of time. The state consists of five averaged orbital elements; the costate consists of the adjoints to these elements. In order to produce trajectories using the maximum rate-of-change of energy strategy, the costate equations were not used. Instead the adjoint to the semimajor axis was set to a nonzero value, and the other adjoints were constrained to be zero. Since the energy is proportional to the negative of the inverse of the semimajor axis, this strategy has the desired result. This strategy is equivalent to forcing the primer vector to be tangent to the orbit at all times. (For the solar sail, this does not mean that the thrust is tangential).

The strategy requires that the energy change be maximized where the energy, E, is given by

$$E = \frac{-u}{a} \frac{m}{2} \qquad \text{(E.1)}$$

Thus

$$\frac{2}{m}\dot{E} = \frac{\mu}{a^2}\dot{a} \qquad (E.2)$$

where m is the mass (constant), μ is the gravitational constant, and a is the semimajor axis. Thus $\dot{E}$ is maximized by maximizing $\dot{a}$. Since the variation of parameters equation for semimajor axis is given by

$$\dot{a} = 2\frac{a^2}{\mu}\underline{V}^T\underline{u} \qquad (E.3)$$

Then a is maximized when $\underline{u}$ has the largest projection onto the velocity vector, $\underline{V}$. For the sail, the thrust direction, $\underline{u}$, will not necessarily be colinear with $\underline{V}$. The above procedure is simply accomplished using the optimization program by constraining the adjoint to semimajor axis to be a non-zero constant and the other adjoints to be zero. The variation of parameters equations for all the orbital elements, $\underline{z}$, can be written (M is a matrix):

$$\dot{\underline{z}} = M\underline{u} \qquad (E.4)$$

Then the Hamiltonian is

$$H = \underline{\lambda}^T\dot{\underline{z}} \qquad (E.5)$$

Then if the adjoint vector is $\underline{\lambda}^T = [k, \underline{0}^T]$, $H = [k, \underline{0}^T]\,\dot{\underline{z}} = k\,\dot{a}$

Thus maximizing H, maximizes $\dot{a}$. Since the optimizing program uses the method of averaging, it is the mean energy rate that is actually maximized.

The thrust vector for the solar sail is calculated as a function of the primer vector (or equivalently, $M^T\underline{\lambda}$). For a flat perfectly-reflecting sail, the force acts normal to the sail and is proportional to $\cos^2\theta$, where θ, the cone angle, is the angle between the normal and the sun - vehicle vector. The relationship between thrust direction and primer vector has been previously derived, for example, in Ref. 6. A more accurate force model for the square sail is given in Ref. 22. In this case the force is proportional to $C_1 + C_2 \cos 2\theta + C_3 \cos 4\theta$, where the cone angle, θ, is the angle between the force direction and the sun-vehicle vector. In this case the calculation of the thrust vector is more involved, but has also been implemented in the SUNSPOT code.

A number of trajectories were generated using the maximum rate-of-change of energy strategy. Different initial orbits were assumed; some cases used the idealized [illegible]il, others the more accurate model; some cases included shadowing. [illegible] case did not include solar motion. Oblateness was not included in any of the cases. A memo describing these cases was sent to the technical monitor[29].

REFERENCES

1. Wiley, C., (pseudonym: Saunders, R.), "Clipper Ships of Space," Astounding Science Fiction, May 1951.

2. Wright, J., and Warmke, J., "Solar Sail Mission Applications," Paper 76-808, AIAA/AAS Astrodynamics Conference, San Diego, California, August, 1976.

3. Sands, N., "Escape from Planetary Gravitational Fields by Use of Solar Sails," ARS Journal, Volume 31, April, 1961, pp. 527-531.

4. Fimple, W.R., "Generalized Three-Dimensional Trajectory Analysis of Planetary Escape by Solar Sail," ARS Journal, Volume 32, June, 1962, pp. 883-887.

5. Zhukov, A.N., and Lebedev, V.N., "Variational Problem of Transfer Between Heliocentric Orbits by Means of a Solar Sail," Cosmic Research, Volume 2, 1964, pp. 41-44.

6. Sauer, C.G., "Optimum Solar-Sail Interplanetary Trajectories," Paper 76-792, AIAA/AAS Astrodynamics Conference, San Diego, California, August, 1976.

7. MacNeil, R.H., "The Heliogyro, An Interplanetary Flying Machine," Astro Research Corp. Report ARC-R-249, March, 1967.

8. Hedgepeth, J.M. and Benton, M.D., "Analysis of Planetary Flyby Using the Heliogyro Solar Sailer", Astro Research Corporation ARC-R-296, August, 1968.

9. MacNeal, R.H., Hedgepeth, J.M. and Schuerch, H.U., "Heliogyro Solar Sailer Summary Report", NASA-CR-1329, June, 1969.

10. MacNeal, R.H., "Structural Dynamics of the Heliogyro, NASA-CR-1745A, 1971.

11. Sackett, L.L., and Edelbaum, T.N., "Effect of Attitude Constraints on Solar-Electric Geocentric Transfers," J. Spacecraft and Rockets, Volume 13, No. 3, March 1976, pp. 174-179.

12. Sackett, L.L., Malchow, H.L., and Edelbaum, T.N., "Solar Electric Geocentric Transfer with Attitude Constraints: Analysis," NASA CR-134927, C.S. Draper Laboratory Report R-901, August 1975.

13. Kryloff, N., and Bogoliuboff, N., Introduction to Non-Linear Mechanics, Princeton University Press, 1947.

14. Broucke, P.A., and Cefola, P.J., "On the Equinoctial Orbital Elements," Celestial Mechanics, Volume 5, No. 3, May 1972, pp. 303-310.

15. Edelbaum, T.N., "Optimal Thrust-Limited Orbit Transfer in Strong Gravitational Fields', Lecture Notes in Mathematics, 132 Symposium on Optimization, Springer Verlag, Berlin, 1970.

16. Edelbaum, T.N., "Optimal Power Limited Orbit Transfer in Strong Gravity Fields", AIAA J., Vol. 3, No. 6, 1965.

17. Cefola, P.J., "Equinoctial Orbit Elements -- Application to Artificial Satellite Orbits", AIAA Paper No. 72-937, Palo Alto, 1972.

18. Uphoff, C., "Numberical Averaging in Orbit Prediction", AIAA Paper No. 72-934, Palo Alto, September 1972.

19. Kaufman, B., "Variation of Parameters and Long-Term Behavior of Planetary Orbiters", AIAA Paper 70-1055, Santa Barbara, August 1970.

20. Jasper, T.P., "Low-Thrust Trajectory Analysis for the Geosynchronous Mission", Paper 73-1073, AIAA 10th Electric Propulsion Conference, Lake Tahoe, Nevada, October-November, 1973.

21. Sackett, L.L., and Edelbaum, T.N., "Optimal Solar Sail Spiral to Escape", AAS/AIAA Astrodynamics Conference, Jackson, Wyoming, September, 1977.

22. Green, A.J., "Optimal Escape Trajectory from a High Earth Orbit by Use of Solar Radiation Pressure" M.I.T., M.S. Thesis, Draper Lab. Report T-652, August 1977.

23. Wright, J., "Solar Sail Force Model," Jet Propulsion Laboratory Interoffice Memorandum 312/77.3-201, March 1977.

24. Cefola, P.J., Long, A.C., Holloway, G., Jr., "The Long-Term Prediction of Artificial Satellite Orbits", AIAA Paper No. 74-170, Washington, D.C., 1974.

25. Jezewski, D.J., and Faust, N.L., "Inequality Constraints in Primer Optimal, N-Impulse Solutions," AIAA Journal, Volume 9, No. 4, April 1971, pp. 760-763.

26. Battin, R.H., Astronautical Guidance, McGraw-Hill, New York, 1964.

27. Melbourne, W.G., et. al., Constants and Related Information for Astrodynamic Calculations, 1968, NASA TR32-1306, JPL, Pasadena, 1968.

28. Escobal, P.R., Methods of Orbit Determination, Wiley, New York, 1965.

29. Sackett, L.L. "A Strategy Which Maximizes Mean Rate-of-Change of Energy for Solar Sail Planetary Escape", Draper Lab. Memo, 16 May 1977.